

# A Northern Survey of Gamma-Ray Blazar Candidates

David Sowards-Emmerd<sup>1</sup>, Roger W. Romani, Peter F. Michelson<sup>1</sup>, Stephen E. Healey<sup>1</sup> & Patrick L. Nolan

*Department of Physics, Stanford University, Stanford, CA 94305*

dse@darkmatter.stanford.edu, rwr@astro.stanford.edu, peterm@stanford.edu, sehealey@stanford.edu, pln@razzle.stanford.edu

## ABSTRACT

In preparation for *GLAST*, we have compiled a sample of blazar candidates to increase the pool of well studied AGN from which *GLAST* counterparts will be drawn. Sources were selected with our Figure of Merit (FoM) ranking; thus, they have radio and X-ray properties very similar to the *EGRET* blazars. Spectroscopic confirmation of these candidates is in progress, and more than 70% of these objects have been identified as flat spectrum radio quasars and BL Lac objects. We present  $\sim 250$  new optical blazar identifications based on McDonald Observatory spectroscopy, 224 with redshifts. Of these, 167 are in our FoM-selected set.

To motivate the  $\gamma$ -ray nature of these objects, we analyzed the current release of the *EGRET* data for possible point sources at their radio positions. We develop two distinct methods to combine multiple *EGRET* observations of a sky position into a single detection significance. We report a detection of the signal of the set of blazar candidates in the *EGRET* data at the  $> 3\sigma$  level by both techniques. We predict that the majority of these blazar candidates will be found by *GLAST* due to its increased sensitivity, duty cycle and resolving power.

## 1. Introduction

The *EGRET* telescope on the Compton Gamma Ray Observatory (*CGRO*) satellite detected 271 sources in a survey of the  $\gamma$ -ray ( $\sim 100$  MeV to 10 GeV) sky. Counterparts for the majority of these sources have remained elusive, and until recently, roughly one quarter of these had been identified as blazars (Hartman et al. 1999; Mattox et al. 2001). By

---

<sup>1</sup>also, Stanford Linear Accelerator Center, Stanford, CA 94039-4349

adopting a new technique, we have now pushed the identified fraction to  $\sim 70\%$  above decl.  $> -40^\circ$ ,  $|b| > 10^\circ$ , excluding the Galactic bulge (Sowards-Emmerd et al. 2003, hereafter SRM03; Sowards-Emmerd et al. 2004). The Large Area Telescope (LAT) on the Gamma-ray Large Area Space Telescope (*GLAST*) satellite, scheduled for launch in early 2007, is predicted to detect over an order of magnitude more blazars than its predecessor. The improved sensitivity and resolving power of the LAT will provide more accurate source positions; however, the fainter sources will still only be localized to 5-10 arcminutes. *GLAST* will be instrumental in verifying the questionable *EGRET* detections but will present an even larger set of its own marginal or unidentified  $\gamma$ -ray detections. The current literature is lacking in well studied sources that would be realistic counterparts for the thousands of new *GLAST* detections.

Blazars are jet-dominated active galaxies viewed close to the axis of a relativistic jet. Blazar emission spans the entire range from radio to  $\gamma$ -rays and is often observed to be highly variable. High-energy emission is thought to be the result of synchrotron self-Compton (SSC) upscattering (Urry & Padovani 1995); additionally, Compton upscattering of seed photons originating outside the jet is often invoked (Bottcher & Dermer 2002).

Under the current classification scheme, blazars are divided into two classes: flat spectrum radio quasars (FSRQs) and BL Lacartae objects (BL Lacs) (Urry & Padovani 1995). According to the current zoology, BL Lacs are a less luminous, more local population, drawn from a parent distribution of elliptical galaxies. FSRQs, drawn from a quasar parent distribution, are generally higher power sources and are visible to much higher redshift. Both classes typically exhibit compact radio cores with flat radio spectra ( $\alpha < -0.5$ , where  $S_\nu \propto \nu^{-\alpha}$ ).

To aid in the counterpart identification of *GLAST* detections, we have created a blazar survey that seeks to identify a number of flat spectrum radio sources comparable to those expected from extrapolation of the 3EG (Hartman et al. 1999) detections. We select targets by applying our Figure of Merit (FoM) analysis, described in detail in SRM03, to objects in the Cosmic Lens All-Sky Survey (CLASS). Excluding known 3EG counterparts, we have compiled a source list of 710  $\gamma$ -ray blazar candidates. The radio and X-ray properties of these sources are very similar to those of the 3EG blazars, and many are as bright or brighter in the radio. As blazars are highly variable in  $\gamma$ -rays, we expect that many of these were simply inactive (in a ‘low state’) when observed by *EGRET*. We have found archival identifications and redshifts for nearly half of these sources in the current literature, and the remainder are being observed at McDonald Observatory. We have contributed 241 new spectroscopic identifications in this paper. This means that this northern sample is currently 74% identified.

To further motivate the blazar nature of the survey sources, we have searched the current release of the *EGRET* data for excess flux at the radio source positions. To this end, we

have developed two methods to rank  $\gamma$ -ray detections statistically in the *EGRET* data. As a reality check on our technique, we calculate the equivalent significance of a subset of the 3EG sources.

The selection criteria of the blazar candidate survey are outlined in Section 2. The methods used to convert the *EGRET* Test Statistic (TS) into a probability for an individual observation and to combine these observations into an overall significance of a  $\gamma$ -ray detection are described in Section 3. In Section 4, these two methods are applied to 3EG sources, survey sources, and the background sky. A discussion of the merits of the two methods also appears there. Section 5 details the spectroscopic observations of survey blazars. Finally, Section 6 presents a rudimentary comparison between the 3EG blazars and the blazar candidates presented in this survey.

## 2. Survey Selection

### 2.1. Figure of Merit Selection

By comparing the properties of radio sources located within 3EG error ellipses (95% confidence contours) to the background distribution, we have developed a new method of ranking counterparts of *EGRET*  $\gamma$ -ray sources. We believe that previous analyses relied too heavily on single dish 6 cm radio fluxes. The recent release of the 8.4 GHz Cosmic Lens All-Sky Survey (CLASS) (Myers et al. 2003) in the north provided uniform coverage over much of the northern sky. In addition to more accurate core fluxes, non-simultaneous one-to-one spectral indices can also be extracted from the CLASS by pairing it with the 1.4 GHz NRAO VLA Sky Survey (NVSS) (Condon et al. 1998). This mitigates the confusion in matching between the older single dish radio surveys and improves the spectral index determination. Fluxes for CLASS sources were assigned by selecting the brightest source in each pointing and combining all the flux within a 1" radius to include any compact jet features. These CLASS sources were matched to the NVSS positions with a 4" match radius. Based on the number of sources in our survey, we expect on the order of one spurious match. Finally, the *ROSAT* All-Sky Survey (RASS) catalogs were also integrated into this data set to provide additional leverage in finding blazars.

Examining these surveys in the context of 3EG, we quantified the correlation between flat spectrum radio sources and 3EG contours (SRM03), which took the form of a fractional excess,  $n$ , of sources (in a given flux or spectral index bin) found within the 3EG positional

95% confidence contours relative to the random background sources:

$$n = \frac{N_{3\text{EG}} - N_{\text{Random}}}{N_{3\text{EG}}} \quad (1)$$

$$\text{FoM} = n_{8.4\text{GHz}} \times n_{\alpha} \times n_{\text{X-ray}} \times \text{Positional Dependence} \quad (2)$$

where these functions are defined as:

$$n_{8.4\text{GHz}} = -3.47 + 2.45\text{Log}_{10}(s_{8.4}) - 0.34[\text{Log}_{10}(s_{8.4})]^2 \quad (3)$$

$$n_{\alpha} = \text{Median}[0, 0.19 - 0.35\alpha_{8.4/1.4}, 0.4] \quad (4)$$

$$n_{\text{X-ray}} = 0.5 + \text{Median}[0, 0.49 + 0.41\text{Log}_{10}(\textit{cps}), 0.5] \quad (5)$$

The full analysis is described in detail in SRM03, including the positional dependence.

Using the FoM method of selecting blazar candidates, we have created a survey tailored to find objects similar to the 3EG blazars. Radio candidates were selected from the 3.5 cm CLASS. In this work, we exclude the positional dependence of the FoM and select objects based only on their intrinsic properties: radio flux, spectral index, and X-ray flux. We have selected sources such that their FoM would meet our original ‘plausible’ (<18% false positives) 3EG FoM limits if the source were located on a 3EG 95% contour. This leaves us with 710 sources selected from the CLASS survey that meet our criteria and were not previously associated with 3EG sources. Properties of these sources are detailed in Table 1, the full version of which is available in the electronic version. The FoM selection effectively imposes a hard minimum on the CLASS radio flux of  $\sim 140$  mJy.

## 2.2. X-ray Selected Sources

Before the CLASS data were available, we selected target sources as an extension of the Deep X-ray Blazar Survey (DXRBS) (Perlman et al. 1998) pushing fainter in radio flux. Sources were selected from NVSS/GB6/RASS matches by the DXRBS criteria (keeping  $\alpha < 0.7$  and relaxing the flux cut). This means that a RASS X-ray detection was required for inclusion in the survey. Application of the FoM technique shows that these sources are not strongly correlated with the 3EG positions. Nevertheless, these sources are generally legitimate blazars, and so we include their spectroscopic properties for comparison. We note here that several of the 3EG blazars previously identified were not detected in the RASS, which in part led us to drop the X-ray detection requirement. Also, for high-power, low-peak blazars (FSRQs), the synchrotron peak is generally in the optical/IR so that the X-ray band, lying between the synchrotron and Compton components, can be quite faint. In contrast, the

higher peak BL Lacs often show bright synchrotron X-rays, but are less luminous in the GeV range. Most of the X-ray selected sample does not make the FoM cut since the radio fluxes are typically much fainter ( $\sim 50$  mJy) than the FoM-selected sources. For completeness, we tabulate redshifts and identifications in Table 2 for the X-ray selected sources that did not meet the FoM criterion. Comparisons between properties of sources selected by this method and by the FoM method are presented in Section 6.

### 3. Analysis of the $\gamma$ -ray Data

To further motivate the  $\gamma$ -ray nature of our blazar candidates, we investigate the possibility that these blazars produce flux detected by *EGRET* but below the 3EG catalog threshold. This is done through a reanalysis of the *EGRET* data products, cleaned of the 3EG sources. We begin with the counts maps (photons), exposure maps, and maps modeling Galactic foreground emissions from the current release of the *EGRET* data products. These maps exist with a wide range of photon energy cuts. For this analysis we follow the standard procedure and only employ the  $E > 100$  MeV data. These data files are divided in time into individual ‘Viewing Periods’ (VPs), which are pointings typically spanning a few days to a few weeks, and into ‘Cycles,’ which comprise roughly a year’s worth of observations. Maps were also produced for all possible sequential combinations of these Cycles.

LIKE (v5.61 at the time of analysis) is the standard source detection routine and was developed specifically for *EGRET* data (Mattox et al. 1996). LIKE computes a ‘Test Statistic’ (TS) value through a maximum likelihood technique that compares the likelihood of detecting a source to the null likelihood (no source) for a given position through fits to the aforementioned data files. Source positions, detection significances and fluxes can be extracted from the likelihood maps created by LIKE by searching for peaks in the maps. Once sources are detected, they can be modeled in the background or ‘cleaned,’ and these ‘cleaned’ maps can be searched again for the peaks in likelihood. This procedure can be iterated down to a fixed TS threshold.

At present, the 3EG catalog represents the most thorough analysis of the *EGRET* data collected during survey mode (Cycles P1-P4). Sources compiled in the 3EG catalog were selected by searching combinations of the *EGRET* data for any  $\sqrt{\text{TS}} \geq 4$  detections ( $\sqrt{\text{TS}} \geq 5$  required for  $|b| < 10^\circ$ ). The blocks of data searched for excess  $\gamma$ -rays using LIKE included VPs, a handful of combinations of sequential VPs, Cycles P1-P4, and the combinations of Cycles P12, P34 and P1234. For a detailed description of the specifics of the 3EG catalog, we refer the reader to Hartman et al. (1999). However, this 3EG detection threshold, required for inclusion in the catalog, does not account for the number

of trials examined – generally on the order of 15-35 – nor does it account for the increase in significance associated with choosing the source position at the local TS maximum instead of using the more accurate radio counterpart position. Additionally, only sequential VPs were coadded and analyzed, although a randomly flaring source might be expected to appear in disjoint VPs.

### 3.1. Searching the *EGRET* Data

From the previous analyses of the *EGRET* data, we believe the  $\gamma$ -ray behavior of these blazars is often highly variable on timescales down to at least the length of *EGRET* VPs. Therefore, we select the individual VPs as the building blocks for our analysis. However, we wish to avoid making any unnecessary assumptions about the  $\gamma$ -ray properties of these sources; that is, we do not want to be limited to searching for sources that exhibit a single flare or, conversely, are steady in the  $\gamma$ -rays.

In our search for correlation between this survey and  $\gamma$ -rays detected by *EGRET*, we chose to examine the significance of  $\gamma$ -ray detections at the precise radio positions of sources. Using radio positions avoids ‘peaking up’ the source positions on background fluctuations. Obviously, this method generally returns a lower significance detection compared to using the position where the TS is a maximum ( $\gamma$ -ray position). Therefore, our detection significance represents a conservative lower limit when compared with the 3EG rankings. We believe this is the proper method for computing the flux or significance of a detection for *EGRET* data when a precise position is known for a candidate counterpart.

### 3.2. Method

We begin by analyzing the individual blocks of data: VPs ( $\sim$ few days), Cycles ( $\sim$ year), and combinations of Cycles. Details of the beginning and ending dates and field centers of the VPs are summarized in Hartman et al. (1999). For each VP overlapping our region of interest, we create likelihood maps from the  $E > 100$  MeV maps using LIKE. All 3EG sources in the field of view of a given viewing period are modeled (fluxes fit, not fixed). Only data within  $30^\circ$  ( $19^\circ$  for the four ‘narrow-mode’ pointings) of the field center are included in the analysis. TS values representing the likelihood of source detection at a given point can be read directly off these  $0.5^\circ \times 0.5^\circ$  gridded maps.

We analyze only the region covered by CLASS ( $0^\circ < \text{decl.} < 75^\circ$  and  $|b| > 10^\circ$ ). Additionally, we remove the Galactic bulge to a radius of  $30^\circ$  from the Galactic center due

to the high density of 3EG detections in the bulge. Finally, regions of  $2^\circ$  radius around 3EG sources were excluded from the analysis. LIKE tends to oversubtract sources when they are modeled, leading to an excess of low TS values relative to a random background; that is, when a point source is modeled by LIKE, the resulting likelihood distribution in that region is not consistent with random background and is instead almost entirely filled with  $TS < 1$  values. If sources were properly cleaned, one would expect to find a random distribution (e.g., approximately one  $TS \geq 4$  ( $2\sigma$ ) point for every  $\sim 40$  points) where a source was modeled. This oversubtraction problem becomes insignificant at approximately  $2^\circ$  from *EGRET* sources. A precise treatment of this issue would involve making cuts around each 3EG source based on its flux in each individual viewing period; however, we believe that a simple  $2^\circ$  cut is satisfactory for the purpose of this work. The subset remaining after applying these cuts contains 578 of the original 710 objects.

### 3.3. Converting TS into a Probability

With TS values in hand, we require a means to transform a set of TS into a meaningful probability of a  $\gamma$ -ray excess at a given position. We consider three approaches to converting TS to a properly normalized probability. The trivial method employed in Mattox et al. (1996) is simply to assume that TS is distributed like  $\chi_1^2/2$ . From this, one can simply convert via  $\sqrt{TS} \rightarrow \sigma$ . This predicts that exactly 50% of the data points in a blank field should have  $TS = 0$ . However, in the northern sky data cleaned of the 3EG sources, even excluding  $2^\circ$  around the positions of the 3EG sources, we find  $\sim 59\%$  of the points have  $TS = 0$ . We believe that this is largely due to overfitting of *EGRET* point sources and the free normalization of the diffuse background flux. This therefore produces a large discrepancy in any analysis that includes low TS values. This method may be reasonable when applied to large TS values; however, in searching for faint detections it is clearly inadequate.

The following two methods treat the cleaned *EGRET* data as the starting point and use the observed distribution of TS values to determine the corresponding probability. This is done by summing up the number of positions in a given VP with TS greater than a given value and normalizing this to the total number of points in the viewing period:  $\text{Prob}( >TS ) = \#(>TS) / \#(\text{Total})$ . This probability function is only applicable to points in a single VP, so this procedure is repeated for each VP and Cycle. The overall number of positions in a VP is the limiting factor here, and due to the spatial cuts listed above, this number can be as small as a few hundred. For small TS values, this method, while heuristic, is the most robust.

To extend the analysis to lower probabilities (larger TS), we can concatenate the VP

TS distributions and compute the probability distribution for all VPs at once. In doing this, we are able to increase the number of points considered by two orders of magnitude, and hence the resulting range of probabilities can be extended by a comparable amount. This approach averages out the VP-to-VP variations in the low-TS end of the distributions. This is checked by comparing with the results of the individual VP method; little difference is observed between the resulting final probabilities for low-significance sources. Thus, as one would expect, the background fluctuations average out in the sets of overlapping VPs. Since these differences do average out, we chose to adopt this method because it allows the larger TS values to be treated uniformly and it extends the probability range by two orders of magnitude. By selecting this occurrence-based method over  $\chi^2$ , we are treating the data as though we are starting from scratch with the 3EG-cleaned maps. Examples of these distributions are shown in Figure 1.



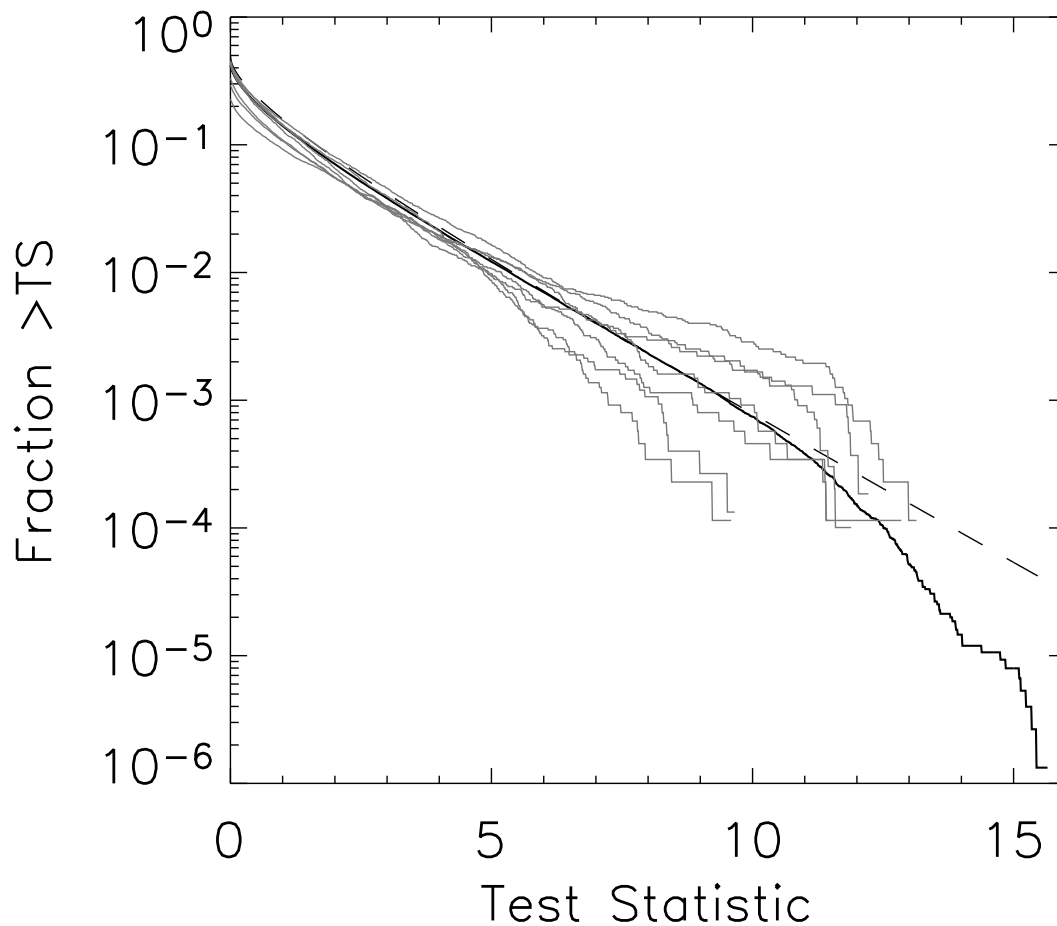


Fig. 1.— The distribution of TS for seven individual VPs (gray) and the concatenation of all 169 VPs (solid black). This may be compared with the  $\chi^2/2$  distribution (dashed black). Note the large discrepancy between these distributions as TS approaches zero. This effect is averaged out in the concatenated distribution. Additionally, note the large variation in the maximum TS values found in individual VPs.

### 3.4. Combining the Information

For each test position, we now have a set of probabilities corresponding to the individual VP observations. Our task now is to integrate these probability estimates into a single detection significance. We investigate two methods. The first method takes an agnostic stance on the temporal behavior of a source and combines all the information available on the VP timescale. We believe that it should be possible to extract almost all of the information available in the Cycle and combination maps by combining information from the individual VPs. We create the ‘combined’ probability at a given position by multiplying the individual VP probabilities in which that position was observed. Clearly, the resulting probability is strongly dependent on the number of VPs, so we must renormalize. We do so by integrating over the volume of  $N$ -dimensional combined probability space where the combined probability is less than or equal to that of the source. That is, we determine how likely it is to build up the combined probability in question from  $N$  observations of random TS values. This problem can be solved analytically, and the final, normalized probability can be written as:

$$P_{\text{norm}} = p \sum_{i=0}^{N-1} (-1)^i \frac{\ln^i p}{i!} \quad (6)$$

where  $p$  is the product of VP probabilities at a given position. Using this procedure, we can compare positions observed in different numbers of viewing periods. We designate this probability as the ‘Product’ probability.

In the second method, for each position, we create a set of TS values extracted from the likelihood maps from VPs, Cycles, and combinations of Cycles (P12, P34, P1234). We include combinations of Cycles in this case because we are searching for the single strongest detection, be it steady or flaring, and discarding the remaining observations. The normalized probability is then calculated by selecting the maximum TS (minimum probability) from this set, converting it into a probability, and then normalizing this probability for the number of trials using the equation:

$$P_{\text{peak}} = 1 - (1 - p_{\text{min}})^N \quad (7)$$

where  $N$  is the number of cases examined, and  $p_{\text{min}}$  is the minimum probability in the set of observations. This procedure, referred to as the ‘Peak’ method, excels at finding sources that were detected strongly in a single viewing period. This is the preferred method for finding blazars if the flaring timescale is comparable to a VP and if they flare only once during the set of observations. This technique corresponds most closely to the standard 3EG analysis.

### 3.4.1. Call for a 4EG Catalog

Based on the *EGRET* analysis carried out in this work, we believe that a fourth *EGRET* catalog is essential to preparation for *GLAST*, due to reprocessing of the data since the creation of the 3EG catalog. In analyzing the current release of the *EGRET* data (assuming 3EG positions for the sources, but re-modeling the fluxes and Test Statistics), we have found several sources that would have been dropped from the list after reanalysis. One particularly bad example is J1227+4302, whose peak detection drops down to  $\sqrt{\text{TS}} = 1.9$ . A dramatic decrease in photons in the vicinity of this source is visible in comparing the current and 3EG  $E > 100$  MeV raw count maps. When comparing the distribution of TS values extracted from the current *EGRET* data products (cossc.gsfc.nasa.gov - 'Current Date' in the old and current maps are 27/8/96 and 27/3/01 respectively) to the 3EG catalog, an overall drop in detection significance is apparent. While the overall exposure in P1234 has increased in the current reprocessing, the counts have decreased in both the  $<100$  MeV and  $>100$  MeV maps. More quantitatively, the counts decreased by 2.3% and 0.6% in the  $>100$  MeV and  $<100$  MeV maps respectively, while the exposure increased by 0.4% and 0.3%. Additionally, improved Galactic foreground emission models may further alter the extracted source list.

## 4. Application of the Method

### 4.1. Low Significance 3EG Sources

As a reality check, we compute the detection significance by both methods for a subset of the 3EG detections. In order to apply these methods to the 3EG sources, we first have to generate TS maps from which these sources are not excluded. We create two sets of these maps: one where 3EG sources with  $\sigma > 4.75$  are 'cleaned' (modeled and removed), and one where  $\sigma > 4.25$  sources have been cleaned. From these maps, we simply read off the TS values for each VP/Cycle at the 3EG positions of the  $\sigma < 4.25$  and  $\sigma < 4.75$  sources. This differs from the traditional *EGRET* method of modeling all sources simultaneously (which we have also done). Note that here the source positions used were the 3EG  $\gamma$ -ray positions, not the positions of radio counterparts, which should increase the apparent significance. The distributions of Peak and Product probabilities for this sample are plotted in Figure 2.

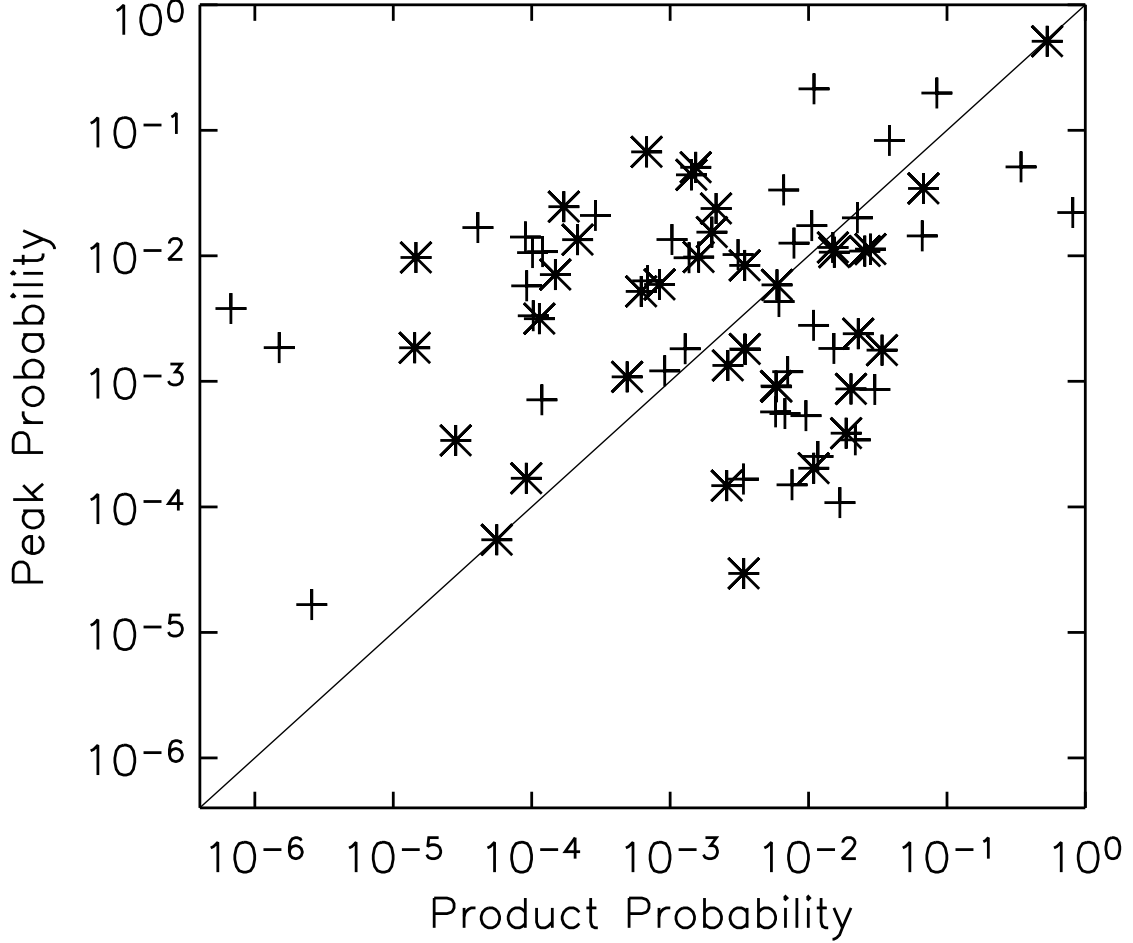


Fig. 2.— The probabilities are plotted for faint 3EG sources for both the Product and Peak methods. Pluses and stars represent  $4.25 < \sqrt{\text{TS}} < 4.75$  and  $\sqrt{\text{TS}} < 4.25$  sources respectively. The threshold for inclusion in the 3EG catalog appears to be  $\sim 2\sigma$  after accounting for the number of trials. Both methods show a wide range of statistical significance, strongly affected by the number of trials. For the selected sources, this dominates the range of the Peak method probability. The two methods exhibit large differences in  $\gamma$ -ray probabilities for individual sources and we believe these methods are complementary. The lowest significance point is J1227+4302, a source whose peak TS dropped from  $\sim 16$  to  $\sim 4$  in the current release of the data.

Since we have correctly normalized for the number of trials, we expect that the probabilities will be significantly lower than the 3EG. The significance threshold of sources in the 3EG catalog is in fact closer to  $2\sigma$  when we account for the number of trials. As noted above, in addition to the decrease in significance due to the normalization process, we also find a systematic drop in TS values for these sources in the current release of the data, arguing that a fourth *EGRET* catalog should be created.

#### 4.2. The 3EG-Cleaned Background Distribution

In order to determine whether the Peak and Product methods produce reasonably normalized probabilities, we created a ‘background sample’ in the form of a grid of  $0.5^\circ \times 0.5^\circ$  pixels spanning  $0^\circ < \text{decl.} < 75^\circ$ ,  $|b| > 10^\circ$  and a minimum of  $2^\circ$  away from modeled 3EG sources. We then filled in this grid with the actual TS values from the VP and Cycle maps. Since we do not model the ‘ $3\sigma$  3EG’ sources or anything fainter, we expect real sources to be present in this background. However, we anticipate that the low-TS values should be distributed as true random background. This is nearly the case for the Product background distribution; however, the Peak background distribution is far from random. Therefore, to compare these methods on equal footing, we must renormalize these probabilities.

We choose to renormalize these probability distributions by renormalizing the background probability distribution to a uniform probability distribution. This is accomplished by computing the occurrence-based probability for survey sources from the background distribution. That is, for a given Peak or Product probability, we total the number of points in the respective background distribution with this probability or lower, divide this by the total number of points in the background, and assign this as our renormalized probability. Because we know that this background includes numerous sources, all of which span tens of pixels, this renormalization produces a very conservative measure of the likelihood of  $\gamma$ -ray detection. In effect, we are calculating the probability that a source is detected more strongly than a random sky position, where the sky contains unmodeled sources.

This procedure would not be necessary if there were no spatial correlations in the data. This is seen through the clustering of  $\text{TS} = 0$  detections seen at a significant fraction of positions on the sky. Of the 61,866 positions ( $0.5^\circ \times 0.5^\circ$  pixels) that we consider in the north, we find that more than 1000 positions have  $\text{TS} = 0$  for every observation. This is a very significant excess over the  $\sim$ dozen such points we would expect to find by chance. We have confirmed via Monte Carlo that combining an arbitrary number of uniformly distributed probabilities by either the Peak or Product method results in a uniform distribution of probabilities, demonstrating that these correlations do exist in the data and are not intrinsic

to the computation methods.

### 4.3. Source Detection

Now that the methods are well understood, we search the *EGRET* data for the FoM-selected blazar candidates. Each technique has its own merits, and we do not deem either method superior. Both the Peak and Product ranking methods produce a significant detection of the blazar candidates above the background. The Peak method excels at finding sources that flare up just once, especially when they sputter around below background for the remainder of the observations. By not including all possible combinations of data – we only include individual VPs, P1, P2, P3, P4, P12, P34, and P1234 – the Peak method misses sources that exhibit multiple flares spanning several cycles (e.g., flaring in P1 and P3). Conversely, the Product method is more efficient at finding sources that are detected multiple times, especially sources where the largest TS is found in P1234. The Product method is much more sensitive to the number of VPs in which a position was observed.

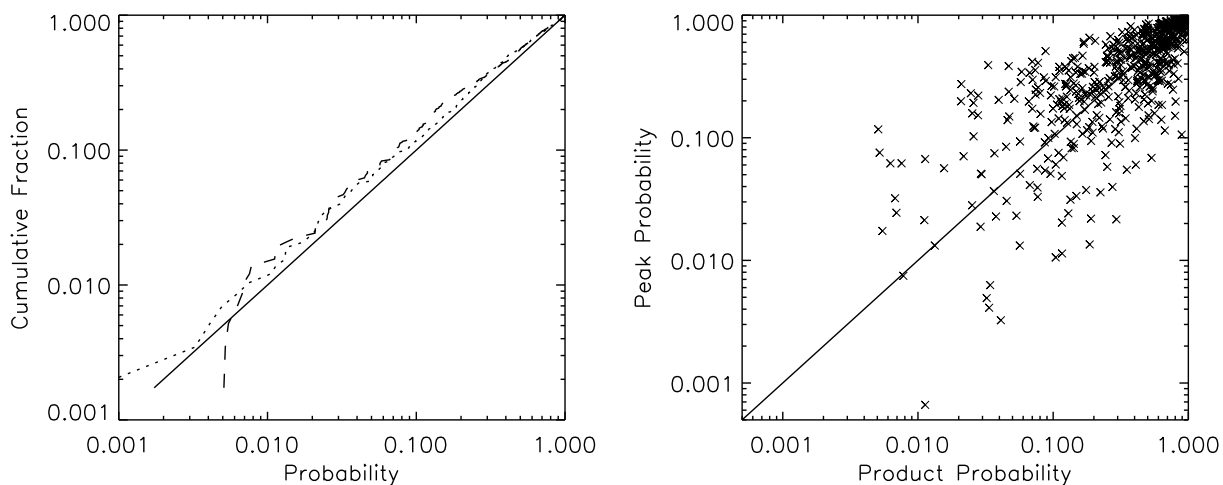


Fig. 3.— Left: The cumulative distribution of probabilities for the Peak method (dotted) and Product method (dashed) are compared to the expected random distribution (solid). Right: Scatter plot contrasting the Peak and Product methods of calculating the  $\gamma$ -ray likelihood. Sources detected with higher significance by the Product method appear above the solid line and those detected more strongly by the Peak method lie below this line. Generally, most sources are best detected by the product method, however a few flaring sources show up best as Peak method detections at the bottom of the plot.

As can be seen in Figure 3, both probability distributions deviate significantly from a uniform random distribution. We quantify this significance in two ways. First, we compare the distribution of probabilities for the blazar candidates computed by each method to the background distribution via the K-S test. The resulting probabilities are 0.00021 ( $3.7\sigma$ ) and 0.0018 ( $3.1\sigma$ ) for the Peak and Product methods respectively.

Second, by setting several detection thresholds, we compile the number of sources selected by each method. These are shown in Table 3. In Table 1, a sample page of the complete table, which is available electronically, the Peak and Product probabilities are tabulated for all sources that survive the spatial cuts.

#### 4.4. Does $\gamma$ -ray Probability Correlate With FoM?

Since we believe that the FoM is selecting *EGRET*-like blazars, we expect a correlation between the FoM and the  $\gamma$ -ray probabilities at a given location. It is unclear whether blazars of comparable radio brightness to the 3EG blazars are not strongly detected because they were not actively flaring in  $\gamma$ -rays during *EGRET* observations or because of a difference in the opening angle of the radio and  $\gamma$ -ray beams. Either of these effects decreases the correlation between the FoM and the  $\gamma$ -ray detection probability. Of course, since these survey sources are typically found to be very faint in  $\gamma$ -rays and background fluctuations are comparable in magnitude, we do not expect to find a strong correlation.

We examine the FoM/ $\gamma$ -ray probability correlation in the data in three ways. First, for each probability scheme, we split the survey data by FoM into two nearly equal parts (at FoM = 0.075) and compare the resulting distributions to the background. In the Peak case, both sets show similar significance in departure from the background as measured by the K-S test: FoM > 0.075  $\rightarrow$  0.034, FoM < 0.075  $\rightarrow$  0.0095. However, for the Product method, the larger FoM set is much more significant: FoM > 0.075  $\rightarrow$  0.0027, FoM < 0.075  $\rightarrow$  0.28.

Alternatively, we compute the Spearman rank correlation for both the Peak and Product methods against the FoM. The resulting coefficients (significances) are -0.07 ( $1.7\sigma$ ) and -0.02 ( $0.54\sigma$ ) for the Product and Peak methods respectively. The correlation has the correct sign for both methods since we expect the smaller probabilities for large FoMs. For the Product method, the correlation is mildly significant; however, for the Peak method, the results are insignificant.

Finally, we create a  $\gamma$ -ray selected subset of the survey by selecting sources detected at the 95% ( $2\sigma$ ) level by either the Peak or Product method and then examining the distributions of corresponding FoM values. Applying this cut, we find 41 sources by the Product



method (34 Peak), and the mean FoM value calculated for these sources is 0.098 (0.089) compared to the average value of 0.083 for the whole survey. Thus  $\gamma$ -ray selection appears to select brighter, flatter radio sources than average, and the Product method is more effective than the Peak method. In all three of the above tests, the strongest correlation is found between the FoM and the Product method.

## 5. Optical Follow-up

Of our 710 survey blazar candidates, nearly half have archival classification and assigned redshifts. Information for these objects was extracted primarily from the Eleventh Edition of the Quasar Catalog (Veron-Cetty et al. 2003) and the Early through 3rd data releases of the Sloan Digital Sky Survey (Abazajian et al. 2004). A handful of objects also appear in the optically bright CLASS Blazar Survey (Caccianiga et al. 2002), the only other blazar survey drawn from CLASS sources. As a follow-up, the remaining positions were queried in the SIMBAD database. The remaining objects are the target of spectroscopic observations at McDonald Observatory.

### 5.1. Hobby-Eberly Telescope/LRS Spectroscopy

Spectroscopic observations were made using the Marcario Low Resolution Spectrograph (LRS) (Hill et al. 1998) on the 9.2 m Hobby-Eberly Telescope (HET) (Ramsey et al. 1998). These targets were observed in regular queue operations from March 2002 to October 2004. Exposures ranged from  $2 \times 300$  s to well over an hour spanning several visits. Image quality generally fell in the range of 1.5" to 2.5". Observations employed a 300 lines  $\text{mm}^{-1}$  grating and a 2" slit for a dispersion of 4 Å per ( $2 \times 2$  binned) pixel and an effective resolution of 16 Å covering approximately  $\lambda\lambda 4200 - 10000$ .

Standard IRAF CCD reductions, calibrations, and optimal extraction were performed. Redshifts were derived whenever possible via cross-correlation analysis with AGN and galactic templates using the IRAF RVSAO package. Images of the extracted 1-D spectra are available online at [astro.stanford.edu/northernblazars.html](http://astro.stanford.edu/northernblazars.html).

We do not yet have spectroscopic data for 186 of the blazar candidates and are still observing these objects with the HET.

## 5.2. 2.7 m/IGI Spectroscopy

A handful of objects were observed with the 2.7 m Harlan J. Smith telescope at McDonald Observatory. Filler observations were made during an observing run from 25-29 July 2003, primarily targeting southern 3EG counterparts. The Imaging Grism Instrument (IGI) spectrograph (Gary Hill) was used with a 6000 Å Grism and a 50 mm lens. A 2" slit was employed for the first 1.5 nights and a 2.5" slit thereafter due to generally poor imaging. The imaging fluctuated around 1.5" to 2" on the best night, but typically held around 2" to 2.5". The IGI setup covered a smaller wavelength range than the HET/LRS, namely  $\lambda\lambda 4250 - 8500$ . Due to a wide range of observing conditions and source brightnesses, total exposures ranged from 300 to 3600 seconds.

## 5.3. Classification

As of this publication, we have obtained 167 new spectroscopic identifications for objects selected by the FoM method. The redshifts and basic properties of these new blazar identifications are listed in Table 1. Sources observed with the HET or 2.7 m were classified based on their observed spectra, S/N permitting. The observed sources fall into the following four categories: BL Lac objects, passive elliptical galaxies, flat spectrum radio quasars, and narrow line radio galaxies. The featureless spectra and spectra with strong absorption lines were segregated into two categories: BL Lac objects and passive elliptical galaxies. BL Lac objects are defined here by the following properties (Marcha et al. 1996): the break contrast  $= \left(\frac{f^+ - f^-}{f^+}\right) < 0.4$ , where  $f^+$  and  $f^-$  are the fluxes redward and blueward of the H/K break, and the rest-frame equivalent width of the strongest emission line detected must be less than 5 Å. The remainder of the absorption line objects are classified as passive elliptical galaxies, although these appear to have active nuclei. For a handful of objects, only narrow emission lines (kinematic width  $< 1000$  km/s) were observed and these were classified as narrow line radio galaxies (NLRG). All other emission line objects were classified as flat spectrum radio quasars.

Archival data were classified based on the source classes of the 11th Veron-Cetty/Veron Quasar Catalogue, Sloan Digital Sky Survey and SIMBAD queries. Objects listed in the Veron catalog as Type 1-1.5 Seyfert galaxies, active galactic nuclei and quasars were classified as flat spectrum radio quasars. Seyfert Type 1.9 and above were classified as narrow line radio galaxies.

#### 5.4. Survey Efficiency

We find that the FoM method is extremely efficient at targeting blazars. In the subset of the sample with reliable identifications, over 95% of sources are identified as FSRQs or BL Lacs. Thus we find a factor of 3 fewer spurious sources by this method than in our X-ray selected pilot survey. Interestingly,  $\sim 25\%$  of the non-blazars found were X-ray detected, suggesting that requiring X-ray detection for an AGN survey is more likely to select NLRGs and passive ellipticals.

#### 5.5. Interesting Spectra

This survey has produced several interesting objects. The most noteworthy is J0906+6930, which we believe to be the highest redshift blazar to date at  $z = 5.47$  (Romani et al. 2004). This is also the highest redshift radio-selected object to date and the brightest object at this redshift at 8.4 GHz. Preliminary 2 cm VLBA snapshots find a jet-like structure, providing more evidence for the blazar nature of this object, and compact flux was also detected at 7 mm at the 40 mJy level.

One FSRQ, J1618+0819, exhibits extremely broad lines ( $\text{FWHM}(v_{kin}) > 17,000$  km/s), where the Balmer lines are clearly multi-peaked, on top of a very strong continuum. J1855+3742, another FSRQ, shows a strong CII line ( $2326 \text{ \AA}$ ) not generally observed in blazars, the equivalent width of which is comparable to that of MgII. Additionally, we find several new bright featureless BL Lac objects. Spectra of these objects are shown in Figure 4.

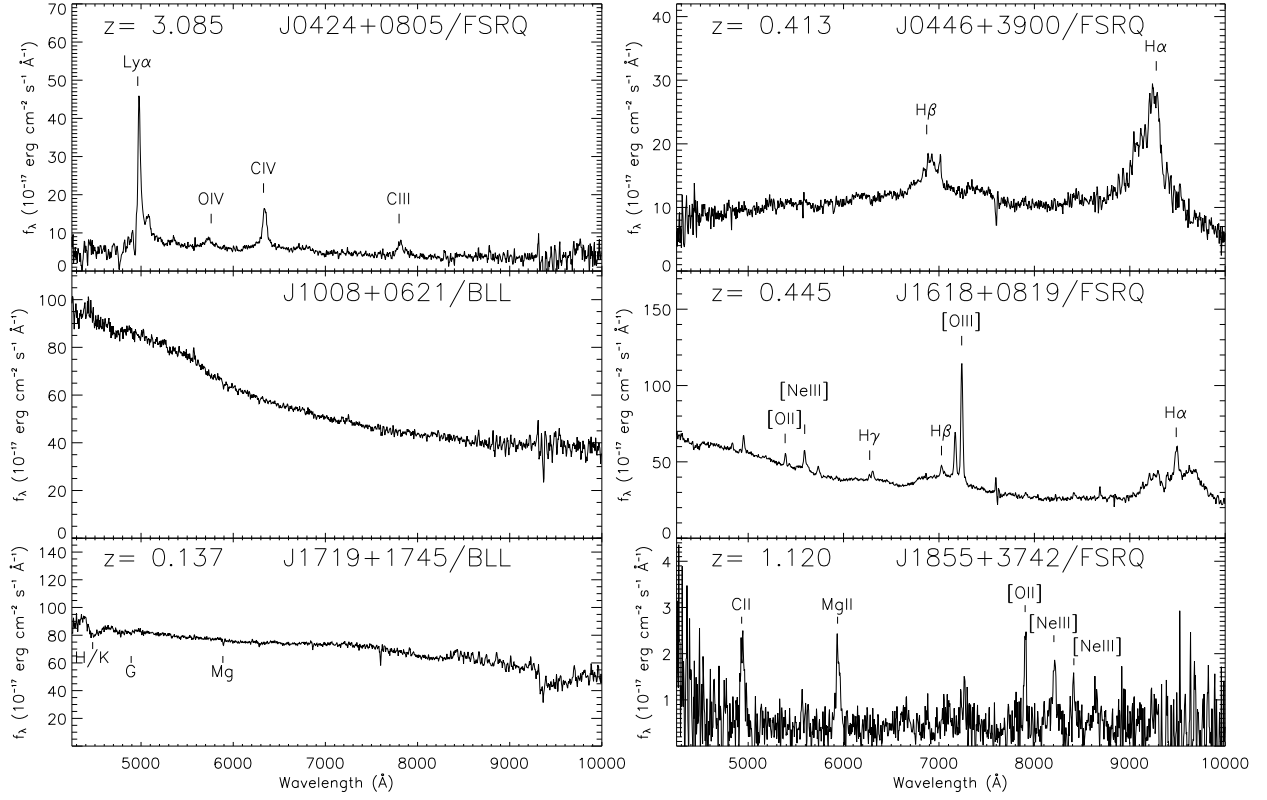


Fig. 4.— Sample Spectra: J0424+0805 – A moderately high redshift FSRQ, J1008+0621 – A typical featureless BL Lac object, J1719+1745 – A source classified as BL Lac in the literature without redshift - we have determined a robust redshift from our new spectroscopy and confirm the BL Lac ID, J0446+3900 and J1618+0819 – FSRQs with extremely broad Balmer lines (multiple components), and J1855+3742 – A weak-continuum FSRQ; note the unusual occurrence of the CII emission line.

## 6. Source Populations

We can now compare this FoM-selected sample with the 3EG sample. We believe that this survey is composed of both a fainter extension of the 3EG as well as sources that would have been detected by *EGRET* had they not been in a low-flux state when observed. We examine the redshift distribution and source population of these samples as well as the effects of X-ray selection.

### 6.1. Redshift Distribution

The primary difference between sources in this sample and the 3EG counterparts is simply the proximity to strong *EGRET*  $\gamma$ -ray detections. The redshift distributions of these two samples are indistinguishable by the K-S test ( $\text{Prob}_{\text{K-S}} = 0.19$ ). For comparison, the redshift histogram of FSRQs from this work is plotted against the distribution of 3EG counterparts (SRM03, SRM04) in Figure 5. Only the FSRQs are considered in this exercise since for the BL Lacs we have a much smaller number of redshifts, and the redshift measurements are much less uniform than in the well observed 3EG sample. The X-ray detected survey sources are on average less distant than the non-X-ray detected sources. The mean redshifts of the FoM survey blazar candidates are 1.08 and 1.52 for the X-ray detected and the non-X-ray detected sources respectively, averaging to 1.37 overall. Our DXRBS-like survey, which required X-ray detections, had an even lower mean redshift of 0.84. The 3EG blazar counterparts fall at a slightly lower redshift of  $z = 1.32$  on average but are consistent with the FoM-selected distribution. Not surprisingly, requiring X-ray detections selects a more local population of sources since the RASS is a relatively shallow survey. The set of blazar candidates detected in the RASS were on average 50% brighter at 8.4 GHz than those not seen in X-rays. Additionally, the X-ray detected FoM-selected blazar candidates are 1.3 magnitudes (USNO B1.0 R2 magnitude)(Monet et al. 2003) brighter optically than the rest. These tend to be ‘high peak’ blazars (HBL) with the synchrotron peak extending to the optical and X-ray Urry & Padovani (1995). These will be relatively low luminosity  $\gamma$ -ray sources.

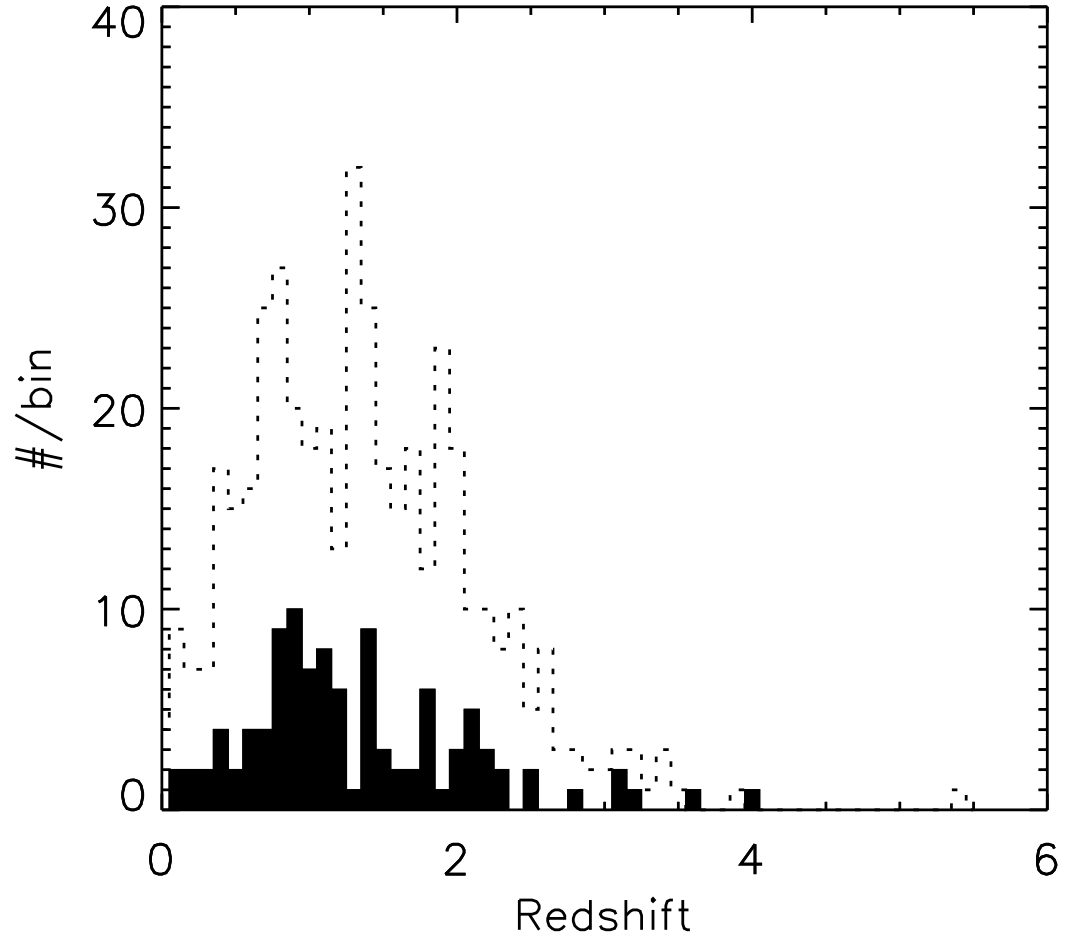


Fig. 5.— Redshift histograms of the 3EG FSRQs (filled) and the survey FSRQs (dotted line). Comparing the two distributions via the K-S test results in a probability of 0.19 that they are drawn from the same parent distribution.

## 6.2. BL Lac Fraction

In the 3EG sample, above decl. =  $-40^\circ$  and away from the Galaxy, we found  $\sim 18\%$  BL Lac objects and  $\sim 78\%$  flat spectrum radio quasars. To date, in the FoM-selected survey we find a lower BL Lac fraction of  $\sim 13.6\%$ . This likely stems from the fact that the 3EG sample is nearly complete, while the FoM sample only has identifications for  $\sim 74\%$  of the sources, where the majority of these IDs are archival. Clearly FSRQs, which generally have very strong emission lines, require lower S/N to make a solid ID and thus are more likely to be identified than BL Lacs.

In the original X-ray selected sample, we found 39% of the objects to be BL Lacs, along with a significantly lower efficiency for finding blazars (86%). In the FoM-selected set, we have classifications for 30 BL Lacs and 143 FSRQs (17.3% BL Lacs) detected in X-rays. The BL Lac fraction is much smaller for sources not detected in the RASS: we find 38 BL Lacs and 288 FSRQs (11.7% BL Lacs). Thus, as expected the X-ray detection criteria select a significantly larger percentage of BL Lac objects.

## 7. Conclusions

We have compiled a survey of 710 objects selected from radio and X-ray data to have properties similar to the 3EG blazar counterparts. Of these objects, we have contributed 167 new spectroscopic identifications along with robust redshifts for the majority. Our spectroscopy represents an improvement of  $\sim 50\%$  over the archival IDs in the northern sky. Because these sources were selected in the same way as the 3EG counterparts but were not detected in the 3EG catalog, we believe that many of these sources were simply in low states during their *EGRET* exposures. However, we cannot rule out the possibility that the differences in the  $\gamma$ -ray and radio beaming may preclude detections of these sources in the GeV range. We introduce two means of statistically ranking *EGRET*  $\gamma$ -ray detections by combining information collected during the survey phase of the mission. Providing further evidence for the blazar nature of these sources, we have convincingly detected the signal of these FoM-selected candidate blazars in the *EGRET* data at the  $\sim 3.5\sigma$  level by both of these methods. However, the FoM for individual sources was only weakly correlated with the significance of excess  $\gamma$ -ray flux.

*GLAST* will help test whether these FoM-selected sources are strong  $\gamma$ -ray emitters. In addition, we expect that *GLAST* will put tighter constraints on the typical duty cycle of blazars. Based on the findings in this work, we also believe that a 4EG catalog needs to be created to adequately model the blazar population in preparation for *GLAST*. Since *GLAST*

will of course produce an all-sky survey, we are extending a CLASS-like VLA survey south of decl. =  $0^\circ$  from which we expect to draw a similar number of  $\gamma$ -ray blazar candidates. Ultimately we seek to identify a nearly uniform all-sky set of 2,000-3,000 blazars to match the expected *GLAST* detections.

DSE and SEH were supported by SLAC under DOE contract DE-AC03-76SF00515, and PFM acknowledges support from NASA contract NAS5-00147.

## REFERENCES

- Abazajian, K. et al. 2004, astro-ph/0410239
- Bottcher, M. & Dermer, C.D. 2002, ApJ, 564, 86
- Caccianiga, A., Marcha, M.J., Anton, S., Mack, K.-H., Neeser, M.J. 2002, MNRAS, 329, 877
- Condon, J.J., et al. 1998, AJ, 115, 1693
- Hartman, R.C., et al. 1999, ApJS, 123, 79
- Hill, G.J., Nicklas, H.E., MacQueen, P.J., Tejada, C., Cobos Duenas, F.J. & Mitsch, W. 1998 Proc. SPIE, 3355, 375
- Marcha, M.J.M., Browne, I.W.A., Impey, C.D., & Smith, P.S. 1996, MNRAS, 281, 425
- Mattox, J.R., et al. 1996, ApJ, 461, 396
- Mattox, J.R., Hartman, R.C., Reimer, O. 2001, ApJS, 135, 155
- Monet, D.G., et al. 2003, AJ, 125, 984
- Myers, S.T., Jackson, N.J., Browne, I.W.A., Bruyn, A.G., Pearson, T.J., Readhead, A.C.S., Wilkinson, P.N., Biggs, A.D., Blandford, R.D., Fassnacht, C.D., Koopmans, L.V.E., Marlow, D.R., McKean, J.P., Norbury, M.A., Phillips, P.M., Rusin, D., Shepherd, M.C., & Sykes, C.M. 2003, MNRAS, 341, 1
- Perlman, E.S., Padovani, P., Giommi, P., Sambruna, R., Jones, L.R., Tzioumis, A. & Reynolds, J. 1998, AJ, 115, 1253
- Ramsey, L.W. et al. 1998, Proc. SPIE, 3352, 34
- Romani, R.W., Sowards-Emmerd, D., Greenhill, L. & Michelson, P.F. 2004, ApJ, 610, L9



Sowards-Emmerd, D., Romani, R.W. & Michelson, P.F. 2003, ApJ, 590, 109

Sowards-Emmerd, D., Romani, R.W., Michelson, P.F. & Ulvestad, J.S. 2004 , ApJ, 609, 564

Urry, C.M. & Padovani, P. 1995, PASP, 107, 803

Veron-Cetty, M.P. & Veron, P. 2003, A&A, 412, 399

Table 1. FoM-selected Objects

Name	FoM	Prod Prob	Peak Prob	S <sub>8.4</sub> (mJy)	$\alpha$	RASS Cnts	R2	z	Type <sup>a</sup>	ID Origin <sup>b</sup>
J000504.36+542824.9	0.106	–	–	382.5	-0.47	0.000	18.2	0.504	F	2
J000520.21+052410.7	0.065	0.489	0.732	228.9	-0.33	0.000	16.2	1.887	F	1
J000557.17+382015.1	0.134	0.044	0.084	1077.6	-0.37	0.000	17.1	0.229	F	1
J000648.78+242236.4	0.051	0.833	0.915	230.9	-0.14	0.000	18.7	–	?	0
J001028.74+204749.7	0.072	0.841	0.836	272.1	-0.31	0.042	18.4	0.600	F	1
J001033.98+172418.7	0.074	0.183	0.370	867.5	0.01	0.055	16.9	1.601	F	1
J001131.90+704531.6	0.073	–	–	657.1	-0.02	0.000	–	–	?	0
J001130.40+005751.8	0.071	0.058	0.345	278.7	-0.28	0.026	20.0	1.492	F	1
J001229.29+470434.6	0.061	0.204	0.215	183.2	-0.49	0.000	20.8	–	?	0
J001247.38+335338.4	0.076	0.931	0.903	213.4	-0.54	0.000	–	–	?	0
J001356.37+191041.9	0.111	0.373	0.527	393.7	-0.50	0.000	18.1	–	B	3
J001708.47+813508.1	0.143	–	–	1361.1	-0.38	0.057	15.9	3.387	F	1
J001751.76+531219.1	0.104	–	–	632.7	-0.27	0.000	18.3	2.574	F	2
J001937.85+202145.5	0.103	0.616	0.642	1232.9	-0.14	0.000	19.7	–	B	5
J001945.78+732730.0	0.098	–	–	1330.7	-0.10	0.000	18.2	1.781	F	1
J002102.81+715020.8	0.053	–	–	250.4	-0.13	0.000	–	–	?	0
J002335.44+445635.7	0.066	0.469	0.585	240.0	-0.31	0.000	–	–	?	0
J002703.29+595852.9	0.072	–	–	193.5	-0.61	0.000	–	–	?	0
J002715.37+224158.1	0.058	0.798	0.873	323.8	-0.07	0.000	15.6	1.119	F	1
J002834.21+240808.1	0.079	0.859	0.897	211.1	-0.63	0.000	18.0	0.373	B	2
J002945.89+055440.6	0.066	0.024	0.231	361.1	-0.11	0.027	19.5	1.314	F	1
J003732.19+080813.0	0.081	0.782	0.793	236.0	-0.52	0.000	–	–	?	0
J003824.84+413706.0	0.111	0.820	0.833	1009.3	-0.22	0.026	18.9	1.353	F	1
J003828.89+185617.7	0.069	0.728	0.560	193.0	-0.56	0.000	19.6	–	?	0
J003939.61+141157.5	0.075	0.516	0.503	369.8	-0.19	0.000	19.8	1.738	B	2
J004204.54+232001.1	0.051	0.202	0.379	906.2	0.17	0.000	19.4	–	?	0
J004219.45+570836.5	0.058	–	–	895.3	0.12	0.000	18.3	1.141	F	1
J004244.37+100949.1	0.051	0.621	0.795	261.8	-0.07	0.000	–	–	?	0
J004700.42+565742.4	0.124	–	–	481.5	-0.53	0.000	18.9	0.747:	F	2
J004937.99+512813.7	0.059	0.210	0.153	226.3	-0.26	0.027	20.7	0.869	F	2
J004943.23+023703.7	0.080	0.643	0.585	525.7	-0.13	0.000	19.0	–	B	5
J005227.82+440254.5	0.051	0.991	0.961	211.1	-0.20	0.000	18.3	2.623	F	2
J005417.62+681111.1	0.066	–	–	271.6	-0.24	0.000	–	–	?	0
J005417.68+705356.5	0.063	–	–	289.4	-0.17	0.000	18.8	–	?	0
J005655.29+162513.3	0.144	0.171	0.168	587.1	-0.87	0.000	19.5	0.206	B	2
J005733.32+221841.3	0.051	0.736	0.829	182.8	-0.33	0.000	19.9	–	?	0
J010038.29+334506.1	0.068	0.414	0.118	199.9	-0.49	0.000	19.1	2.143	F	2
J010245.76+582411.1	0.129	–	–	1426.8	-0.29	0.000	17.3	0.644	F	2
J010549.92+481903.1	0.075	0.006	0.024	784.2	-0.01	0.000	–	–	?	0
J010610.96+253930.4	0.078	0.753	0.580	260.8	-0.40	0.000	14.9	–	?	0
J010633.35+130002.6	0.058	0.421	0.587	263.1	-0.16	0.000	–	–	?	0
J010747.88+261108.6	0.079	0.655	0.644	318.8	-0.30	0.000	–	0.522	F	2
J010838.77+013500.3	0.077	0.329	0.295	2263.2	0.06	0.021	19.0	2.099	F	1
J011137.31+390628.0	0.134	0.280	0.572	873.9	-0.41	0.000	–	0.669	N	1
J011205.82+224438.7	0.105	0.320	0.498	493.4	-0.15	0.151	15.4	–	B	5
J011212.94+352219.3	0.054	0.364	0.627	379.7	0.01	0.049	18.0	0.450	F	1

Table 1—Continued

Name	FoM	Prod Prob	Peak Prob	S <sub>8.4</sub> (mJy)	$\alpha$	RASS Cnts	R2	z	Type <sup>a</sup>	ID Origin <sup>b</sup>
J011327.00+494824.0	0.051	0.204	0.617	528.9	0.11	0.057	17.8	0.389	F	1
J011638.06+242253.7	0.062	0.153	0.228	209.1	-0.37	0.000	–	–	?	0
J011725.20+141812.4	0.051	0.894	0.818	227.3	-0.16	0.000	20.2	–	?	0
J012129.91+112700.5	0.080	0.359	0.295	214.1	-0.86	0.000	16.7	2.465	F	2
J012141.59+114950.4	0.129	0.519	0.403	1865.0	-0.26	0.000	18.6	0.570	F	1
J012238.81+250231.7	0.071	0.308	0.158	699.8	-0.00	0.000	17.9	2.025	F	1
J012425.82+561851.9	0.053	–	–	340.0	-0.00	0.000	19.0	2.364	F	2
J012642.79+255901.2	0.066	0.480	0.481	871.6	0.06	0.052	17.8	2.358	F	1
J012808.06+490105.9	0.090	0.066	0.339	369.0	-0.33	0.000	12.1	0.067	F	1
J013027.63+084246.2	0.056	0.116	0.020	264.4	-0.13	0.000	19.8	0.725	F	2
J013126.71+383439.2	0.056	0.621	0.585	245.4	-0.17	0.000	–	–	?	0
J013220.45+562040.3	0.058	–	–	406.1	-0.00	0.000	–	–	?	0
J013244.12+432532.6	0.063	0.897	0.842	239.6	-0.27	0.000	19.1	–	?	0
J013658.59+475129.1	0.120	0.085	0.311	1644.0	-0.21	0.000	19.2	0.859	F	1
J013708.73+312235.7	0.064	0.945	0.963	434.5	-0.03	0.000	–	–	?	2
J014303.18+412920.4	0.058	0.641	0.864	253.1	-0.18	0.000	19.3	0.824	F	2
J014824.37+385405.2	0.055	0.293	0.021	350.8	-0.01	0.000	17.5	1.442	F	1
J014922.37+055553.5	0.109	0.850	0.816	1223.4	-0.18	0.000	–	2.344	F	1
J014949.71+185720.5	0.095	0.092	0.099	469.2	-0.28	0.000	18.4	0.584	F	2
J015127.14+274441.7	0.093	0.114	0.194	1052.8	-0.09	0.000	20.4	1.260	F	1
J015218.05+220707.7	0.078	0.498	0.314	1008.4	0.00	0.000	18.8	1.320	F	1
J015558.93+223011.8	0.053	0.757	0.709	280.7	-0.07	0.000	19.6	1.456	F	2
J020201.65+394321.5	0.051	0.451	0.672	175.1	-0.36	0.000	–	0.780	F	1
J020243.65+420516.3	0.116	0.586	0.692	415.9	-0.52	0.000	18.8	–	B	3
J020333.38+723253.6	0.058	0.966	0.964	281.3	-0.13	0.000	14.8	–	B	5
J020504.92+321230.0	0.069	0.156	0.199	637.8	0.00	0.000	17.4	1.466	F	1
J020514.00+393256.9	0.059	0.452	0.471	163.8	-0.67	0.000	18.1	0.454	F	2
J020951.79+722926.6	0.054	0.951	0.922	549.6	0.09	0.000	17.1	0.895	F	1
J021113.17+105134.7	0.062	–	–	357.6	-0.07	0.000	15.4	–	?	0
J021310.53+182025.4	0.118	0.168	0.583	371.3	-0.66	0.000	19.7	1.817	F	2
J021717.12+083703.8	0.053	0.885	0.967	323.2	-0.02	0.053	14.6	–	?	0
J021730.81+734932.6	0.090	0.625	0.447	2292.8	-0.01	0.038	18.9	2.367	F	1
J021748.95+014449.6	0.121	0.134	0.311	1178.9	-0.26	0.000	18.5	1.715	F	1
J021907.02+012059.8	0.081	0.151	0.380	576.1	-0.11	0.000	19.5	1.623	F	1
J022850.05+672103.0	0.103	–	–	1806.2	-0.10	0.000	18.1	0.523	F	2
J023045.70+403253.0	0.086	0.962	0.978	581.1	-0.15	0.000	18.5	1.019	F	1
J023145.89+132254.7	0.097	0.885	0.990	1751.1	-0.07	0.000	17.9	2.059	F	1
J023307.94+390523.7	0.076	0.779	0.931	203.5	-0.62	0.000	17.5	2.024	F	2
J023714.03+052649.9	0.083	0.683	0.881	313.6	-0.35	0.000	18.5	0.561	F	2
J023721.84+302259.8	0.059	0.770	0.246	200.8	-0.36	0.000	–	–	?	0
J023951.26+041621.4	0.075	0.627	0.817	863.9	0.00	0.000	17.3	0.978	F	1
J024005.25+421622.5	0.064	0.586	0.330	176.4	-0.58	0.000	18.5	1.700	F	2
J024229.17+110100.7	0.067	0.077	0.408	1369.0	0.09	0.000	19.6	2.680	F	2
J024918.01+061951.9	0.079	0.687	0.885	579.3	-0.10	0.000	17.5	1.881	F	2
J025134.53+431515.8	0.079	0.558	0.588	1174.1	0.01	0.027	13.7	1.310	F	1
J025137.34+722655.8	0.063	0.343	0.261	191.9	-0.47	0.000	–	–	?	0

Table 1—Continued

Name	FoM	Prod Prob	Peak Prob	S <sub>8.4</sub> (mJy)	$\alpha$	RASS Cnts	R2	z	Type <sup>a</sup>	ID Origin <sup>b</sup>
J025424.71+234326.5	0.111	0.344	0.531	330.4	-0.97	0.000	19.7	1.987	F	2
J025701.34+655635.4	0.058	–	–	253.1	-0.18	0.000	–	–	?	0
J025745.62+184705.3	0.065	0.508	0.380	210.3	-0.40	0.000	19.5	–	B	3
J025850.52+054108.0	0.066	0.109	0.143	243.6	-0.31	0.000	19.4	1.380	F	2
J030222.73+533146.4	0.092	–	–	361.8	-0.37	0.000	18.5	–	?	0
J030335.24+471616.2	0.132	–	–	1616.3	-0.29	0.000	17.0	0.475	B	1
J030548.19+052331.5	0.062	0.885	0.990	200.7	-0.41	0.000	–	–	?	0
J030903.62+102916.3	0.153	0.509	0.854	1157.8	-0.48	0.029	19.9	0.863	F	1
J031049.87+381453.8	0.105	0.528	0.533	460.2	-0.38	0.000	19.2	0.816	F	1
J031243.60+013317.5	0.061	0.695	0.893	453.4	-0.00	0.000	18.0	0.664	F	1
J031301.96+412001.1	0.162	0.480	0.393	670.9	-0.36	0.184	14.5	0.136	F	1
J031948.16+413042.1	0.092	0.970	0.974	34295.6	-0.23	0.000	11.0	0.017	F	1
J031951.25+190131.3	0.096	0.534	0.569	576.4	-0.23	0.000	17.7	0.296	N	2
J032251.83+394802.2	0.104	0.944	0.955	299.2	-0.68	0.000	–	–	?	0
J032520.30+465506.6	0.081	–	–	361.4	-0.26	0.000	–	–	?	0
J032759.21+004422.7	0.050	0.496	0.624	236.5	-0.11	0.000	17.8	1.357	F	1
J033453.31+080014.4	0.082	0.328	0.348	431.5	-0.20	0.000	–	–	?	0
J034328.95+362212.4	0.084	–	–	626.1	-0.11	0.000	19.7	1.484	F	1
J034506.41+145349.5	0.130	0.956	0.865	689.8	-0.44	0.000	20.0	1.556	F	2
J034918.74+460959.6	0.066	–	–	810.2	0.05	0.000	19.1	1.853	F	2
J035430.01+464318.7	0.063	–	–	669.0	0.05	0.000	19.0	–	?	0
J035721.60+231953.8	0.093	0.954	0.962	351.2	-0.39	0.000	18.7	–	?	2
J035746.12+054231.2	0.072	0.481	0.658	224.9	-0.44	0.000	19.2	2.163	F	4
J035902.64+600522.0	0.069	–	–	857.7	0.04	0.031	–	–	?	0
J035927.93+275824.0	0.078	0.473	0.411	208.6	-0.61	0.000	–	1.157	F	2
J035944.91+322047.0	0.088	0.039	0.203	778.5	-0.11	0.000	19.8	1.331	F	2
J040111.74+031828.6	0.096	0.134	0.245	267.0	-0.98	0.000	20.1	1.524	F	2
J040119.91+041334.4	0.071	0.111	0.378	224.4	-0.43	0.000	–	0.306	E	2
J040145.16+211028.6	0.082	0.753	0.681	379.4	-0.24	0.000	20.3	0.834	F	2
J040305.58+260001.5	0.061	0.806	0.752	786.4	0.08	0.000	–	2.109	F	1
J040922.00+121739.8	0.103	0.051	0.208	667.3	-0.25	0.000	18.2	1.020	B	1
J041245.94+185637.0	0.080	0.678	0.552	339.3	-0.27	0.000	–	–	?	0
J041437.25+341851.1	0.051	0.523	0.382	1314.6	0.20	0.011	–	–	?	0
J041556.52+445249.6	0.078	–	–	286.3	-0.35	0.000	19.4	0.485	N	2
J041819.34+545715.3	0.058	–	–	250.2	-0.18	0.000	–	–	?	0
J041922.54+395528.9	0.104	–	–	655.7	-0.26	0.000	15.4	–	?	0
J042244.39+532426.2	0.065	–	–	548.7	0.00	0.000	–	1.273	F	2
J042252.21+021926.9	0.109	0.308	0.194	975.0	-0.21	0.000	19.4	2.277	F	1
J042457.60+080517.3	0.075	0.310	0.171	270.6	-0.34	0.000	–	3.085	F	2
J042746.04+413301.0	0.072	–	–	653.4	-0.01	0.000	–	–	?	0
J042805.81+325951.9	0.138	0.544	0.239	520.9	-0.71	0.015	19.0	–	?	0
J042835.63+173223.5	0.057	–	–	245.7	-0.19	0.000	18.0	3.317	F	2
J043311.09+052115.6	0.088	–	–	2105.2	0.26	1.705	10.0	0.033	F	1
J043558.37+292336.4	0.084	–	–	254.8	-0.49	0.000	–	–	?	0
J043917.77+304507.5	0.065	0.767	0.789	303.1	-0.17	0.000	–	–	?	0
J044331.63+344106.6	0.091	–	–	798.1	-0.12	0.000	–	–	?	0

Table 1—Continued

Name	FoM	Prod Prob	Peak Prob	S <sub>8.4</sub> (mJy)	$\alpha$	RASS Cnts	R2	z	Type <sup>a</sup>	ID Origin <sup>b</sup>
J044611.49+390017.1	0.136	–	–	502.6	-0.66	0.000	18.4	0.413	F	2
J044835.16+362931.4	0.054	–	–	268.7	-0.11	0.000	–	–	?	0
J044923.30+633209.4	0.070	0.077	0.256	472.2	-0.07	0.000	–	0.781	F	1
J045118.70+593532.1	0.145	–	–	598.7	-0.76	0.000	–	–	?	0
J045242.60+123624.6	0.057	–	–	193.2	-0.36	0.000	19.1	1.176:	F	2
J050145.27+135607.2	0.074	0.220	0.285	372.3	-0.18	0.000	–	–	?	0
J050145.78+712833.9	0.071	0.948	0.883	231.4	-0.41	0.000	–	–	?	0
J050233.21+133810.9	0.119	0.220	0.285	904.7	-0.30	0.000	19.2	–	B	5
J050321.19+020304.6	0.050	0.929	0.735	1469.9	0.21	0.000	–	0.584	N	1
J050356.44+660031.5	0.054	0.056	0.093	199.7	-0.28	0.000	19.8	1.695	F	2
J050842.36+843204.5	0.091	–	–	460.6	-0.26	0.000	18.1	1.340	B	1
J050925.96+054135.3	0.093	0.466	0.325	702.4	-0.16	0.042	15.1	–	B	5
J051002.37+180041.5	0.075	0.631	0.140	720.8	-0.02	0.000	19.0	0.416	F	1
J051138.31+135719.1	0.058	0.066	0.197	465.6	0.02	0.000	18.8	1.695	F	2
J051751.34+064803.1	0.055	0.406	0.446	555.0	0.08	0.033	19.1	0.840	F	2
J051803.82+205452.4	0.119	–	–	451.7	-0.51	0.000	20.4	2.579	F	2
J052732.70+033131.4	0.066	0.351	0.054	327.8	-0.15	0.000	18.4	–	B	5
J053238.99+073243.3	0.091	0.456	0.579	2763.4	-0.01	0.000	17.5	1.254	F	2
J053620.23+503826.2	0.098	–	–	934.9	-0.14	0.000	17.5	–	?	0
J053942.36+143345.5	0.155	–	–	1061.4	-0.51	0.000	–	2.690	F	2
J054116.17+531224.8	0.090	0.805	0.197	780.9	-0.11	0.000	18.2	1.275	F	1
J055217.93+375425.2	0.088	–	–	509.3	-0.20	0.000	18.2	0.815	F	2
J055250.10+031327.2	0.071	–	–	653.7	-0.00	0.000	18.7	–	?	0
J055400.80+685754.4	0.053	0.124	0.262	180.6	-0.36	0.000	19.6	1.372	F	2
J055530.80+394849.1	0.189	–	–	7428.6	-0.90	0.044	17.5	2.365	F	1
J055913.39+580403.4	0.083	0.930	0.504	511.7	-0.16	0.000	19.0	0.904	F	1
J060309.12+174216.8	0.060	–	–	454.1	0.00	0.000	19.1	1.738	F	2
J060550.85+403008.0	0.074	–	–	780.8	-0.00	0.000	20.1	–	?	0
J060723.25+473946.9	0.062	0.835	0.537	403.4	-0.04	0.000	16.3	–	?	0
J060752.67+672055.4	0.093	0.277	0.532	598.8	-0.20	0.024	20.2	1.970	F	1
J061357.69+130645.4	0.077	–	–	602.5	-0.07	0.000	19.4	0.745	F	2
J061808.20+462016.2	0.085	0.988	0.786	227.7	-0.74	0.000	19.6	0.607	F	2
J062317.81+224135.7	0.077	–	–	297.3	-0.31	0.000	–	–	?	0
J062328.93+383049.7	0.062	0.256	0.262	187.3	-0.48	0.000	19.3	0.421	N	2
J062419.02+385648.7	0.054	0.464	0.716	642.0	0.11	0.021	19.2	3.469	F	1
J062603.00+820225.5	0.059	–	–	596.2	0.06	0.000	18.5	0.710	F	1
J063230.78+320053.6	0.079	0.727	0.744	212.0	-0.85	0.000	19.2	1.831	F	2
J063755.94+332206.2	0.066	0.057	0.050	204.3	-0.44	0.000	–	–	?	0
J063802.87+593322.2	0.125	0.863	0.927	575.6	-0.46	0.000	–	–	?	0
J063921.96+732458.0	0.058	0.754	0.794	733.1	0.10	0.000	18.2	1.850	F	1
J064204.25+675835.5	0.107	0.501	0.740	419.7	-0.44	0.000	16.0	3.180	F	1
J064258.13+350918.3	0.052	0.119	0.069	188.8	-0.31	0.000	18.2	0.269	N	2
J064453.71+391447.5	0.093	0.223	0.035	616.2	-0.19	0.000	19.4	1.266	F	1
J064632.02+445116.5	0.188	0.661	0.625	2258.4	-0.91	0.000	18.6	3.408	F	1
J065031.25+600144.5	0.112	0.979	0.966	766.5	-0.28	0.000	19.6	0.455	F	1
J065048.19+561634.4	0.062	0.246	0.245	273.3	-0.18	0.000	19.7	1.427	F	2

Table 1—Continued

Name	FoM	Prod Prob	Peak Prob	S <sub>8.4</sub> (mJy)	$\alpha$	RASS Cnts	R2	z	Type <sup>a</sup>	ID Origin <sup>b</sup>
J065358.28+370540.6	0.093	0.025	0.158	954.3	-0.11	0.000	18.0	1.982	F	1
J065422.08+504223.9	0.073	0.164	0.107	305.0	-0.25	0.000	15.2	–	?	0
J065423.71+451423.5	0.059	0.317	0.135	392.9	-0.02	0.000	19.7	0.933	F	1
J065510.02+410010.1	0.087	0.680	0.588	378.6	-0.30	0.000	9.37	0.021	N	1
J065705.67+242355.3	0.061	0.638	0.185	360.0	-0.06	0.000	19.3	1.925	F	2
J065917.99+081330.9	0.069	–	–	821.8	0.03	0.000	16.1	–	?	0
J070001.52+170921.7	0.151	–	–	1398.9	-0.43	0.000	16.0	–	?	0
J070231.79+264411.0	0.054	0.796	0.443	441.2	0.05	0.000	–	–	?	0
J071243.63+503322.6	0.102	0.178	0.115	396.3	-0.42	0.000	18.6	–	?	0
J071751.85+453803.2	0.094	0.736	0.733	562.4	-0.22	0.000	17.5	0.940	F	1
J072123.91+040644.2	0.113	–	–	585.0	-0.36	0.024	17.0	–	?	0
J072201.26+372228.6	0.061	0.294	0.321	234.7	-0.26	0.000	17.2	1.629	F	1
J072210.03+284220.6	0.061	0.629	0.342	168.3	-0.82	0.000	–	–	?	0
J072448.40+030825.1	0.060	–	–	230.0	-0.26	0.000	–	–	?	0
J072516.80+142513.7	0.088	0.149	0.129	1148.1	-0.05	0.000	17.4	–	?	0
J072550.63-005456.5	0.074	–	–	1244.8	0.04	0.000	15.8	0.127	B	1
J072614.26+215320.0	0.159	0.561	0.158	813.0	-0.67	0.031	17.9	–	?	0
J072611.74+791131.0	0.098	–	–	711.8	-0.20	0.000	–	–	?	0
J072820.60+215306.3	0.176	0.942	0.938	1359.6	-0.60	0.000	17.7	–	?	0
J072849.63+570124.3	0.098	0.881	0.860	644.3	-0.21	0.000	14.8	0.426	F	1
J073051.34+404950.8	0.055	0.662	0.623	368.9	-0.00	0.000	16.5	2.501	F	1
J073133.74+245158.5	0.051	0.817	0.587	321.0	-0.00	0.000	19.4	–	?	0
J073352.52+502209.0	0.071	0.575	0.474	734.2	0.00	0.000	18.3	0.720	F	1
J073502.31+475008.4	0.071	0.195	0.110	460.5	-0.08	0.059	16.9	0.782	F	1
J073658.07+260449.8	0.050	0.683	0.883	277.2	-0.04	0.000	18.4	–	?	0
J073918.03+013704.6	0.076	0.274	0.039	1710.8	0.06	0.000	16.1	0.190	F	1
J074033.54+285247.2	0.075	0.765	0.432	199.5	-0.65	0.000	19.1	0.711	F	1
J074110.70+311200.2	0.130	0.190	0.094	3366.5	-0.23	0.000	16.2	0.631	F	1
J074202.75+490015.6	0.078	0.073	0.356	491.8	-0.12	0.000	–	–	?	0
J074533.06+101112.6	0.060	0.243	0.072	2534.4	0.16	0.000	–	–	?	0
J074559.32+331334.1	0.050	0.670	0.114	196.4	-0.25	0.034	18.0	0.610	F	1
J074640.43+273459.0	0.074	0.779	0.332	361.8	-0.19	0.015	–	–	?	0
J074714.62+763917.2	0.140	–	–	547.5	-0.80	0.000	–	–	?	0
J074836.10+240024.1	0.147	0.936	0.814	1541.6	-0.28	0.096	17.8	0.409	F	1
J075000.33+182311.4	0.089	0.681	0.434	337.1	-0.36	0.000	18.9	–	?	0
J075020.43+481453.5	0.077	0.045	0.030	748.3	-0.03	0.016	18.3	1.951	F	1
J075032.87+102126.7	0.067	0.134	0.031	254.6	-0.28	0.000	–	1.116:	F	2
J075052.04+123104.8	0.118	0.147	0.341	1967.9	-0.19	0.000	17.1	0.889	F	1
J075240.90+373024.3	0.067	0.998	0.990	223.9	-0.38	0.000	20.2	0.440	F	1
J075301.38+535259.6	0.116	–	–	1196.9	-0.23	0.035	16.7	0.200	B	1
J075448.85+303355.0	0.082	0.534	0.200	215.9	-0.86	0.067	18.0	0.796	F	1
J075654.61+634759.0	0.061	0.897	0.911	268.0	-0.19	0.000	–	–	?	0
J075706.64+095634.8	0.143	0.257	0.214	1363.5	-0.23	0.113	15.9	0.660	B	1
J080248.03+180949.2	0.086	0.698	0.405	633.7	-0.13	0.000	–	–	?	0
J080518.17+614423.7	0.067	0.956	0.876	725.7	0.03	0.000	19.6	3.033	F	2
J080633.47+450432.2	0.057	0.388	0.592	403.0	0.00	0.000	19.3	2.102	F	1

Table 1—Continued

Name	FoM	Prod Prob	Peak Prob	S <sub>8.4</sub> (mJy)	$\alpha$	RASS Cnts	R2	z	Type <sup>a</sup>	ID Origin <sup>b</sup>
J080816.48+731511.9	0.052	0.782	0.650	307.9	-0.02	0.000	–	–	?	0
J080839.66+495036.5	0.059	–	–	880.0	0.11	0.000	16.2	1.432	F	1
J080856.65+405244.8	0.142	0.399	0.760	1181.8	-0.40	0.042	16.6	1.418	F	1
J081058.99+413402.7	0.052	0.303	0.628	257.7	-0.09	0.026	18.4	0.507	F	1
J081303.84+254211.0	0.061	0.791	0.672	429.2	-0.01	0.000	18.8	2.024	F	1
J081439.19+643122.0	0.077	0.613	0.671	221.6	-0.52	0.000	16.8	–	?	0
J081525.94+363515.1	0.069	0.939	0.869	885.1	0.04	0.000	18.4	1.028	F	1
J081815.99+422245.4	0.077	0.073	0.121	1041.2	0.01	0.025	17.8	0.530	B	1
J081902.33+322637.2	0.063	0.795	0.946	272.8	-0.19	0.000	20.0	0.651	F	4
J082447.23+555242.6	0.103	0.676	0.773	1736.1	-0.10	0.000	17.8	1.417	F	1
J082455.48+391641.9	0.076	0.543	0.249	1251.1	0.07	0.082	17.2	1.216	F	1
J082538.61+615728.5	0.085	0.454	0.301	628.0	-0.13	0.063	17.0	0.542	F	1
J082550.33+030924.5	0.145	0.504	0.782	1873.4	-0.18	0.132	14.5	0.506	B	1
J083155.09+084743.6	0.084	0.196	0.260	243.8	-0.53	0.000	19.5	0.940	F	2
J083353.88+422401.8	0.124	0.303	0.218	560.8	-0.46	0.065	16.4	0.249	F	1
J083417.54+601947.0	0.089	0.122	0.380	349.7	-0.35	0.015	19.5	0.720	F	1
J083615.79+005259.9	0.079	0.766	0.874	210.2	-1.23	0.000	–	1.826:	F	2
J083622.89+272852.5	0.109	0.676	0.403	565.5	-0.34	0.018	19.0	0.765	F	1
J083740.24+245423.1	0.070	–	–	541.6	-0.03	0.027	17.4	1.122	F	1
J083949.19+031953.8	0.063	0.339	0.446	615.5	0.04	0.000	–	1.570	F	1
J083949.61+010426.7	0.098	0.621	0.644	620.3	-0.22	0.000	18.5	1.123	F	1
J084957.98+510828.9	0.066	0.230	0.124	335.1	-0.14	0.000	17.7	0.584	F	1
J085135.93+552834.4	0.055	0.618	0.287	194.5	-0.33	0.000	17.8	–	B	5
J085441.99+575729.9	0.062	0.437	0.257	892.5	0.09	0.021	17.4	1.318	F	1
J085656.69+173947.7	0.056	0.295	0.425	158.4	-0.92	0.000	20.1	–	?	0
J090021.43+410822.9	0.058	0.097	0.264	313.4	-0.08	0.000	19.6	1.621	F	4
J090111.86+044858.8	0.095	0.572	0.562	266.3	-0.59	0.000	20.1	1.863	F	1
J090219.28+540257.2	0.060	0.226	0.193	242.3	-0.23	0.000	19.1	–	?	0
J090230.92+431014.1	0.059	0.587	0.590	363.4	-0.04	0.000	19.7	2.410	F	1
J090353.16+675722.7	0.082	0.619	0.725	640.6	-0.09	0.014	18.3	1.499	F	1
J090541.76+284928.2	0.055	0.037	0.022	255.6	-0.14	0.000	19.0	1.219	F	1
J090630.74+693030.8	0.058	0.348	0.535	188.1	-0.40	0.000	–	5.404	F	2
J090855.92+160954.7	0.052	0.202	0.284	235.9	-0.14	0.000	19.2	–	?	2
J090910.09+012135.6	0.076	0.469	0.205	765.8	-0.02	0.058	17.0	1.024	F	1
J090939.84+020005.2	0.056	0.613	0.299	228.2	-0.22	0.000	18.6	–	B	5
J091908.78+332441.9	0.086	0.962	0.948	333.2	-0.35	0.000	–	–	B	3
J092136.23+621552.1	0.127	0.188	0.224	1532.0	-0.27	0.000	18.9	1.446	F	1
J092314.45+384939.9	0.056	0.056	0.013	375.7	-0.00	0.000	–	–	?	0
J092549.96+165812.2	0.062	0.932	0.990	193.4	-0.44	0.000	16.9	–	?	0
J092703.01+390220.8	0.271	0.076	0.032	9176.5	-0.65	0.237	15.9	0.695	F	1
J092824.13+444604.8	0.053	–	–	228.9	-0.17	0.000	18.0	1.904	F	1
J092915.44+501335.9	0.106	0.419	0.280	747.8	-0.21	0.075	15.9	–	B	5
J092943.02+861221.2	0.053	–	–	211.0	-0.23	0.010	18.5	–	B	5
J093055.27+350337.6	0.059	0.488	0.367	460.0	0.01	0.053	18.8	–	B	5
J093406.67+392632.1	0.050	0.169	0.196	188.3	-0.27	0.000	–	–	B	5
J093712.32+500852.0	0.121	0.550	0.478	372.5	-0.46	0.107	18.8	0.276	F	1

Table 1—Continued

Name	FoM	Prod Prob	Peak Prob	S <sub>8.4</sub> (mJy)	$\alpha$	RASS Cnts	R2	z	Type <sup>a</sup>	ID Origin <sup>b</sup>
J093949.61+414154.1	0.053	0.142	0.089	277.8	-0.08	0.000	18.1	1.224	F	1
J094014.72+260329.9	0.059	0.641	0.631	442.9	0.00	0.000	18.9	0.498	?	1
J094148.11+272838.8	0.050	0.626	0.406	227.0	-0.14	0.000	–	–	?	0
J094203.91+640311.3	0.056	0.609	0.842	171.2	-0.49	0.000	19.6	0.952	F	2
J094317.22+170218.9	0.054	0.570	0.558	309.6	-0.04	0.000	–	–	?	0
J094319.15+361452.0	0.112	0.104	0.060	335.2	-0.84	0.039	8.59	0.022	F	1
J094855.34+403944.5	0.069	0.029	0.018	1323.2	0.08	0.031	17.8	1.249	F	1
J094857.32+002225.5	0.084	0.046	0.384	226.8	-0.67	0.040	18.1	0.585	F	1
J095227.30+504850.6	0.065	0.468	0.136	189.6	-0.52	0.014	17.7	1.091	F	1
J095232.02+351252.3	0.050	0.186	0.013	319.6	0.00	0.000	19.4	1.875	F	1
J095327.95+322551.4	0.051	0.155	0.211	199.3	-0.24	0.000	16.7	1.570	F	1
J095649.87+251516.0	0.133	0.544	0.591	1786.8	-0.29	0.047	17.9	0.712	F	1
J095819.67+472507.8	0.108	0.953	0.946	879.6	-0.22	0.066	18.3	1.882	F	1
J095837.80+503957.4	0.065	0.582	0.369	236.6	-0.31	0.000	20.1	1.154	F	1
J100110.20+291137.5	0.070	0.937	0.765	296.0	-0.23	0.023	16.3	–	?	0
J100111.94+342450.4	0.053	0.053	0.023	250.1	-0.12	0.000	19.8	0.948	F	2
J100741.49+135629.6	0.081	0.932	0.973	963.0	-0.02	0.000	18.5	2.706	F	1
J100800.81+062121.2	0.091	0.474	0.398	657.1	-0.16	0.045	16.7	–	B	3
J101015.77+825014.4	0.055	–	–	450.0	0.04	0.000	17.6	0.322	F	1
J101051.82+333017.7	0.068	0.071	0.123	353.3	-0.14	0.000	20.0	2.067	F	2
J101216.39+231214.6	0.072	0.036	0.074	260.0	-0.33	0.000	19.7	0.748	F	2
J101349.61+344550.7	0.057	0.220	0.254	363.8	-0.02	0.000	19.3	1.414	F	1
J101353.42+244916.4	0.147	0.292	0.161	1063.0	-0.45	0.000	15.8	1.636	F	1
J101504.13+492600.7	0.052	–	–	252.2	0.21	1.942	14.5	0.200	B	1
J101538.01+672844.4	0.052	0.131	0.185	150.1	-0.77	0.000	–	–	?	0
J101544.02+122707.0	0.074	0.391	0.672	296.7	-0.27	0.000	18.9	–	B	3
J101644.32+203747.2	0.107	0.021	0.070	1017.7	-0.19	0.000	18.6	3.110	F	1
J101725.88+611627.4	0.094	0.249	0.411	582.7	-0.21	0.000	17.8	2.805	F	1
J101810.98+354239.4	0.084	0.662	0.754	704.0	-0.09	0.033	17.6	1.226	F	1
J101827.85+053029.9	0.053	0.435	0.506	299.3	-0.05	0.000	20.0	1.944	F	4
J101950.87+632001.6	0.090	0.074	0.247	272.7	-0.51	0.000	18.9	–	B	3
J102117.47+343721.6	0.073	0.381	0.371	511.5	-0.07	0.000	17.3	1.404	F	1
J102213.13+423925.6	0.060	0.499	0.791	257.8	-0.19	0.000	–	–	?	0
J102444.80+191220.4	0.067	0.195	0.134	642.8	0.01	0.065	16.4	0.827	F	1
J102556.28+125349.0	0.119	0.685	0.824	910.5	-0.29	0.000	18.9	0.663	F	1
J102745.03+183138.7	0.064	0.721	0.721	173.4	-0.75	0.000	18.9	–	?	0
J102820.40+025522.4	0.056	0.429	0.289	312.2	-0.06	0.000	–	–	?	0
J103322.06+393551.0	0.080	0.097	0.134	509.5	-0.14	0.000	–	1.095	F	1
J103351.42+605107.3	0.056	0.027	0.152	430.4	0.02	0.000	20.2	1.401	F	1
J103632.98+220312.2	0.075	0.612	0.408	364.2	-0.19	0.042	19.0	0.594	F	2
J104117.16+061016.9	0.076	0.630	0.854	1293.8	0.03	0.000	16.1	1.270	F	1
J104309.03+240835.4	0.133	0.332	0.328	685.4	-0.42	0.074	16.4	0.560	B	1
J104423.06+805439.4	0.100	–	–	1020.8	-0.12	0.070	18.2	1.260	F	1
J104552.73+062436.4	0.115	0.374	0.812	400.6	-0.53	0.000	17.5	1.509	F	1
J104827.62+714335.9	0.132	0.136	0.421	1284.5	-0.32	0.000	17.4	1.150	F	1
J105101.37+202719.9	0.111	0.020	0.198	331.4	-0.68	0.000	19.2	1.035	F	2



Table 1—Continued

Name	FoM	Prod Prob	Peak Prob	S <sub>8.4</sub> (mJy)	$\alpha$	RASS Cnts	R2	z	Type <sup>a</sup>	ID Origin <sup>b</sup>
J105148.79+211952.3	0.075	0.036	0.036	1159.5	0.03	0.035	17.7	1.299	F	1
J105653.62+701145.8	0.118	0.158	0.332	607.2	-0.39	0.000	19.3	2.492	F	1
J105811.53+811432.6	0.128	–	–	571.4	-0.49	0.025	18.1	0.706	F	1
J105829.60+013358.8	0.104	0.418	0.289	3582.0	-0.08	0.000	16.6	0.888	F	1
J105939.04+205721.9	0.091	0.006	0.032	284.0	-0.49	0.000	18.9	0.400	F	1
J110214.28+275708.6	0.058	0.476	0.504	286.2	-0.11	0.000	19.6	1.861	F	1
J110313.30+301442.6	0.072	0.646	0.540	248.7	-0.37	0.062	17.1	0.380	F	1
J111609.97+082922.0	0.069	0.793	0.868	329.4	-0.17	0.000	–	0.486	F	1
J111857.30+123441.7	0.118	0.214	0.188	1577.0	-0.21	0.043	19.1	2.117	F	1
J111942.82+041027.9	0.060	0.704	0.276	339.9	-0.07	0.022	19.5	–	?	0
J111952.42+165656.9	0.078	0.382	0.650	217.3	-0.56	0.000	19.0	–	?	0
J112229.71+180526.3	0.058	0.309	0.434	589.8	0.07	0.032	16.8	1.040	F	1
J112402.71+233645.8	0.056	0.587	0.646	472.7	0.04	0.000	19.7	–	B	3
J112542.29+000101.4	0.063	–	–	173.0	-1.01	0.000	17.5	1.696	F	1
J112553.71+261019.9	0.085	0.591	0.295	992.6	-0.04	0.000	18.3	2.341	F	1
J112736.52+055532.0	0.050	0.402	0.205	217.1	-0.17	0.000	19.4	2.217	F	1
J112740.13+565014.7	0.070	0.412	0.230	497.7	-0.06	0.000	20.1	2.890	F	1
J112758.86+362028.3	0.079	0.908	0.627	300.5	-0.33	0.000	20.0	–	?	0
J112813.34+592514.7	0.115	0.491	0.269	581.4	-0.38	0.000	–	1.795	F	2
J112845.55+103906.9	0.091	0.700	0.482	246.7	-1.36	0.000	–	–	?	0
J113053.28+381518.5	0.098	0.116	0.011	910.4	-0.15	0.038	19.4	1.733	F	1
J113626.40+700927.3	0.066	0.529	0.660	213.7	0.06	4.532	10.5	0.046	B	1
J113627.34+340739.5	0.066	0.486	0.289	238.8	-0.32	0.000	–	1.332	F	2
J114306.03+184342.8	0.054	0.780	0.395	142.2	-0.53	0.120	17.4	0.374	F	1
J114341.60+663331.2	0.082	0.413	0.686	275.7	-0.41	0.000	19.2	2.328	F	1
J114626.91+584834.2	0.097	0.755	0.596	565.0	-0.24	0.000	19.3	1.982	F	1
J114658.29+395834.3	0.107	0.072	0.120	575.7	-0.31	0.000	18.5	1.088	F	1
J114759.76+263542.3	0.079	0.743	0.755	447.0	-0.16	0.052	17.0	0.867	F	1
J114850.35+592456.3	0.071	0.550	0.577	521.7	-0.05	0.000	11.5	0.011	G	1
J114856.57+525425.3	0.145	0.104	0.311	597.9	-1.04	0.019	16.4	1.633	F	1
J115019.21+241753.8	0.069	0.911	0.869	745.7	0.02	0.000	15.8	0.200	B	1
J115312.49+805829.1	0.078	–	–	1267.1	0.02	0.000	18.5	1.250	F	1
J115323.97+583138.5	0.087	0.116	0.048	186.8	-0.77	0.133	17.0	0.201	F	4
J115756.13+552712.9	0.072	0.305	0.111	157.2	-0.28	0.628	10.4	0.003	N	1
J115826.77+482516.2	0.090	0.096	0.222	438.6	-0.27	0.000	19.8	2.028	F	1
J120329.85+480313.6	0.149	0.207	0.247	415.2	-1.09	0.110	16.9	0.813	F	1
J120712.62+121145.8	0.088	0.670	0.565	344.1	-0.35	0.000	19.0	0.895	F	1
J120727.90+275458.8	0.062	–	–	544.5	0.02	0.028	18.6	2.177	F	1
J120922.78+411941.3	0.108	0.547	0.255	485.1	-0.33	0.077	16.7	–	B	5
J120945.09+254703.7	0.071	0.967	0.950	456.8	-0.08	0.033	18.9	1.435	F	2
J121459.91+082922.5	0.051	0.270	0.091	262.0	-0.08	0.000	19.8	2.359	F	2
J121503.97+165437.9	0.077	0.190	0.021	400.1	-0.18	0.039	18.9	1.132	F	2
J121711.01+583526.2	0.067	0.033	0.391	482.9	-0.04	0.000	19.1	2.552	F	1
J121752.08+300700.6	0.072	–	–	334.9	0.16	2.779	13.4	0.130	B	1
J121910.58+634410.7	0.086	0.448	0.752	230.5	-0.74	0.000	–	–	?	0
J121906.41+482956.1	0.077	0.173	0.344	667.7	-0.05	0.000	19.9	1.076	F	1

Table 1—Continued

Name	FoM	Prod Prob	Peak Prob	S <sub>8.4</sub> (mJy)	$\alpha$	RASS Cnts	R2	z	Type <sup>a</sup>	ID Origin <sup>b</sup>
J121935.79+660031.8	0.097	0.900	0.681	270.0	-0.72	0.000	19.1	1.266	F	1
J122008.29+343121.7	0.063	0.126	0.132	314.1	-0.14	0.038	17.0	0.130	B	1
J122059.23+380855.6	0.051	0.787	0.686	256.0	-0.09	0.000	–	1.108:	F	2
J122222.54+041315.7	0.117	0.057	0.284	1021.7	-0.15	0.101	17.0	0.965	F	1
J122755.72+493256.0	0.050	0.005	0.017	262.3	-0.06	0.000	19.8	1.348:	F	2
J122847.42+370612.0	0.142	0.801	0.837	868.6	-0.46	0.024	–	1.515	F	1
J123014.09+251807.1	0.100	0.195	0.240	326.4	-0.17	0.248	14.7	0.135	B	1
J123802.44+072321.8	0.080	0.290	0.381	433.2	-0.18	0.000	19.9	1.172	F	2
J123924.59+073017.2	0.090	0.070	0.418	707.3	-0.14	0.049	17.9	0.400	F	1
J124251.37+375100.0	0.078	0.694	0.612	613.4	-0.07	0.000	18.7	1.316	F	1
J124345.03+744237.1	0.107	0.421	0.505	407.4	-0.45	0.031	18.0	0.782	F	1
J124818.78+582028.7	0.117	0.005	0.117	324.4	-0.16	0.515	15.1	–	B	5
J125438.25+114105.8	0.053	0.451	0.391	630.7	0.12	0.062	16.7	0.870	F	1
J125531.75+181750.9	0.075	0.268	0.489	488.9	-0.10	0.013	18.8	1.366	F	2
J130028.53+283010.2	0.057	0.817	0.643	239.9	-0.20	0.000	16.1	0.648	F	1
J130252.46+574837.6	0.155	0.011	0.021	861.5	-0.56	0.024	20.6	–	?	0
J130603.34+552943.8	0.072	0.148	0.033	250.1	-0.36	0.019	18.5	1.601	F	1
J130823.70+354637.1	0.120	0.615	0.840	527.0	-0.45	0.029	19.4	1.055	F	1
J130909.75+555738.1	0.056	0.200	0.340	299.2	-0.08	0.000	17.8	1.629	F	1
J130933.93+115424.5	0.068	0.185	0.654	785.1	0.03	0.000	18.1	–	B	5
J131028.50+004408.8	0.051	0.129	0.024	224.2	-0.16	0.000	19.5	1.603	F	1
J131028.66+322043.7	0.152	0.503	0.516	3061.0	-0.35	0.068	17.9	0.996	F	1
J131053.58+465352.2	0.112	0.839	0.904	355.9	-0.57	0.000	19.7	–	?	0
J131059.40+323334.4	0.108	0.341	0.259	620.6	-0.30	0.017	19.0	1.650	F	1
J131103.20+551354.3	0.075	0.104	0.010	498.2	-0.09	0.000	20.4	0.924	F	1
J131341.65+102714.3	0.060	0.716	0.388	185.2	-0.46	0.000	18.8	–	?	0
J131443.82+530627.7	0.058	0.086	0.091	295.8	-0.10	0.000	–	–	?	0
J131736.49+342515.9	0.068	0.521	0.472	541.3	-0.02	0.044	19.0	1.050	F	1
J132351.57+794251.8	0.068	–	–	593.9	-0.00	0.000	20.3	1.970	F	1
J132952.86+315411.0	0.080	0.076	0.039	850.8	-0.03	0.000	19.7	–	B	3
J133042.59+520215.4	0.052	–	–	171.9	-0.40	0.000	20.6	–	?	0
J133245.24+472222.6	0.105	0.080	0.232	457.5	-0.38	0.028	18.5	0.667	F	4
J133307.49+272518.4	0.095	0.966	0.627	399.2	-0.34	0.000	19.5	–	?	0
J133521.96+454238.2	0.102	0.213	0.263	463.1	-0.35	0.000	17.6	2.450	F	1
J133525.92+584400.2	0.145	0.876	0.909	747.9	-0.52	0.000	–	–	?	0
J133716.05+653246.3	0.051	0.940	0.918	248.5	-0.10	0.000	19.6	0.944	F	4
J133749.64+550102.1	0.051	0.882	0.797	559.1	0.11	0.024	18.2	1.099	F	1
J134208.37+270930.6	0.056	0.622	0.512	298.6	-0.08	0.044	16.8	1.190	F	1
J134345.95+660225.7	0.143	0.954	0.958	595.8	-0.59	0.012	18.8	0.766	F	1
J134723.48+183537.5	0.058	0.398	0.384	374.9	-0.02	0.024	19.5	–	?	0
J134934.65+534117.0	0.050	0.983	0.940	764.3	0.16	0.045	17.0	0.979	F	1
J135022.13+094010.6	0.060	0.585	0.711	250.4	0.06	0.359	12.4	0.132	F	1
J135055.71+642856.8	0.099	0.830	0.780	376.0	-0.41	0.000	–	–	?	0
J135052.73+303453.5	0.142	–	–	671.7	-0.42	0.091	18.8	0.713	F	2
J135116.92+083039.8	0.063	0.300	0.505	389.3	-0.06	0.000	17.6	–	?	0
J135158.19+554210.9	0.066	0.984	0.698	198.9	-0.47	0.000	19.3	–	B	5

Table 1—Continued

Name	FoM	Prod Prob	Peak Prob	S <sub>8.4</sub> (mJy)	$\alpha$	RASS Cnts	R2	z	Type <sup>a</sup>	ID Origin <sup>b</sup>
J135323.15+753257.7	0.120	–	–	384.4	-0.60	0.000	17.7	–	?	0
J135755.37+764321.0	0.080	–	–	715.7	-0.06	0.000	20.2	–	?	0
J135938.09+401138.2	0.080	0.929	0.916	297.8	-0.34	0.000	17.0	0.406	F	4
J135959.70+143633.1	0.073	0.106	0.186	196.2	-0.63	0.000	18.7	1.334	F	2
J140145.70+583542.2	0.050	0.606	0.354	204.3	-0.21	0.000	–	1.923	F	2
J140412.12-001325.1	0.054	–	–	436.2	0.04	0.000	18.8	1.217	F	1
J140501.12+041535.7	0.071	0.892	0.106	868.0	0.03	0.000	19.2	3.215	F	1
J140653.84+343337.2	0.070	0.347	0.638	275.3	-0.28	0.000	18.0	2.556	F	1
J140700.39+282714.6	0.167	0.592	0.508	1936.3	-0.49	0.000	10.2	0.076	F	1
J141035.07+073121.4	0.083	0.531	0.753	335.1	-0.32	0.000	19.5	–	?	0
J141236.37+133438.1	0.065	0.029	0.050	281.2	-0.20	0.000	–	–	?	0
J141509.91+083205.3	0.094	0.477	0.225	259.5	-0.61	0.000	18.6	–	?	0
J141558.81+132023.7	0.119	0.121	0.187	1564.3	-0.21	0.000	18.3	0.246	B	1
J141946.59+542314.7	0.219	0.041	0.003	2248.1	-0.62	0.103	19.2	0.153	B	1
J141959.30+270625.5	0.074	0.402	0.099	338.4	-0.22	0.057	19.4	0.536	F	2
J142020.88+170329.1	0.089	0.720	0.350	242.2	-0.80	0.000	20.0	1.854	F	2
J142123.07+464547.9	0.062	0.691	0.784	209.2	-0.37	0.000	18.0	1.668	F	1
J142230.37+322310.4	0.089	0.485	0.532	527.9	-0.18	0.069	19.1	0.685	F	1
J142306.15+480210.8	0.058	0.834	0.904	399.3	-0.00	0.000	19.9	2.200	F	1
J142314.18+505537.2	0.077	0.245	0.414	214.7	-0.14	0.374	14.9	0.276	F	1
J142549.01+142456.9	0.082	0.508	0.316	586.1	-0.12	0.000	19.5	0.780	F	1
J143009.73+104326.8	0.159	0.798	0.151	837.8	-0.60	0.000	18.6	1.710	F	1
J143040.58+364903.8	0.072	–	–	273.5	-0.30	0.000	19.6	0.564	B	1
J143439.79+195200.7	0.106	0.364	0.241	656.7	-0.27	0.000	19.0	1.382	F	2
J143535.40+301224.5	0.062	0.234	0.118	309.0	-0.13	0.000	–	–	?	0
J143640.98+232103.2	0.058	0.970	0.974	650.7	0.08	0.000	19.2	1.544	F	2
J143645.80+633637.8	0.072	0.821	0.860	872.6	0.02	0.037	16.2	2.062	F	1
J143908.90+211450.8	0.078	0.864	0.742	207.0	-0.62	0.000	–	–	?	0
J143946.97+495805.4	0.078	0.147	0.268	244.6	-0.45	0.014	18.7	0.174	G	1
J144611.64+194526.5	0.050	0.969	0.971	150.5	-0.56	0.000	–	–	?	0
J144635.34+172107.5	0.076	0.111	0.205	714.4	-0.03	0.033	19.0	0.102	F	2
J144828.77+760111.6	0.100	–	–	376.3	-0.42	0.000	–	0.899	F	1
J145031.16+091027.9	0.091	0.308	0.595	502.6	-0.23	0.000	20.1	2.611	F	2
J145301.48+103617.2	0.055	0.766	0.851	242.7	-0.16	0.000	19.1	2.269	F	2
J145353.60+264833.4	0.091	0.965	0.960	671.9	-0.15	0.000	20.0	–	B	3
J145608.11+504836.3	0.053	0.263	0.409	259.2	-0.10	0.000	–	0.480	B	1
J145738.12+074954.7	0.096	0.318	0.392	423.6	-0.33	0.000	19.3	1.838:	F	2
J145844.79+372021.6	0.088	0.299	0.538	370.8	-0.31	0.000	19.4	0.333	B	1
J145935.45+444207.9	0.072	0.294	0.601	216.2	-0.48	0.000	19.8	3.401	F	2
J145958.43+333701.7	0.135	0.378	0.520	327.6	-1.72	0.122	16.9	0.644	F	1
J150048.65+475115.5	0.105	0.245	0.574	678.0	-0.26	0.000	19.6	–	?	0
J150424.97+102939.2	0.081	0.025	0.102	1686.8	0.02	0.000	18.9	1.839	F	1
J150506.47+032630.8	0.136	0.007	0.061	847.6	-0.43	0.000	17.7	0.409	F	1
J150609.52+373051.1	0.081	0.224	0.228	948.8	-0.02	0.000	20.1	0.671	N	1
J150624.75+831928.0	0.057	–	–	260.5	-0.15	0.000	18.8	–	?	0
J150644.11+493355.7	0.070	0.126	0.216	217.4	-0.45	0.000	–	1.397:	F	2

Table 1—Continued

Name	FoM	Prod Prob	Peak Prob	S <sub>8.4</sub> (mJy)	$\alpha$	RASS Cnts	R2	z	Type <sup>a</sup>	ID Origin <sup>b</sup>
J151141.26+051809.2	0.134	0.145	0.448	489.1	-1.17	0.000	13.9	0.084	F	1
J151640.21+001501.8	0.101	0.408	0.060	956.6	-0.12	0.078	10.5	0.052	N	1
J151656.79+193213.0	0.089	0.872	0.916	609.3	-0.16	0.000	17.5	0.650	B	1
J151717.15+133224.4	0.072	0.936	0.927	233.7	-0.41	0.000	–	1.499	F	2
J152149.61+433639.2	0.128	0.163	0.333	547.3	-0.50	0.018	18.8	2.180	F	1
J152209.99+314414.4	0.088	0.496	0.629	493.8	-0.21	0.000	19.8	1.487	F	2
J152642.87+665054.6	0.106	0.865	0.931	305.7	-0.71	0.009	17.2	3.020	F	1
J153552.03+495739.0	0.068	0.424	0.351	306.0	-0.20	0.000	18.6	1.121	F	1
J153916.17+310407.6	0.084	0.365	0.533	231.5	-0.57	0.000	–	–	?	0
J153939.14+274438.2	0.069	0.812	0.629	291.5	-0.23	0.000	17.2	2.190	F	2
J154405.65+324048.3	0.062	0.881	0.861	260.0	-0.21	0.000	16.9	1.047	F	1
J154502.82+513500.8	0.075	0.674	0.762	635.1	-0.04	0.034	17.5	1.930	F	1
J154855.10+172740.9	0.055	0.868	0.592	196.2	-0.32	0.000	20.0	1.873	F	2
J154917.46+503805.7	0.145	0.371	0.472	1286.1	-0.40	0.047	18.1	2.175	F	1
J154929.43+023701.1	0.100	0.121	0.139	918.7	-0.08	0.093	15.5	0.414	F	1
J155035.26+052710.4	0.055	0.714	0.842	1614.6	0.18	0.000	19.0	1.422	F	1
J155158.20+580644.4	0.075	0.609	0.793	305.3	-0.28	0.036	15.6	1.319	F	1
J155543.04+111124.3	0.195	0.020	0.274	506.5	-0.28	1.513	13.9	0.360	B	1
J155751.43-000150.4	0.115	–	–	1552.0	-0.19	0.000	18.7	1.772	F	1
J155930.97+030448.2	0.062	0.629	0.844	415.8	-0.03	0.000	–	3.891	F	1
J160207.26+332653.0	0.067	0.942	0.974	2338.1	0.12	0.000	–	1.000	N	1
J160239.63+264605.9	0.092	0.310	0.496	252.2	-1.08	0.029	17.2	0.372	N	4
J160341.93+110548.6	0.095	–	–	374.3	-0.37	0.000	16.6	–	?	0
J160437.35+571436.6	0.063	0.359	0.729	485.3	-0.00	0.034	17.7	0.720	F	1
J160533.04+300129.7	0.061	0.625	0.433	259.4	-0.20	0.000	19.9	2.404	F	2
J161042.02+241449.0	0.071	0.543	0.639	405.1	-0.12	0.000	19.2	1.449	F	2
J161637.55+045932.7	0.126	0.286	0.316	678.1	-0.42	0.031	19.4	–	?	0
J161749.91+024643.0	0.095	0.864	0.828	783.6	-0.15	0.000	17.1	1.339	F	1
J161826.93+081950.7	0.083	0.175	0.037	249.3	-0.37	0.093	15.9	0.445	F	2
J161914.82+224747.8	0.094	0.803	0.927	649.5	-0.18	0.000	20.0	1.987	F	2
J162031.22+490153.2	0.051	0.076	0.055	401.3	0.06	0.000	17.8	1.513	F	1
J162304.52+662401.0	0.084	0.301	0.307	302.8	-0.38	0.028	16.3	0.203	F	1
J162358.24+074130.5	0.070	0.011	0.000	217.0	-0.44	0.054	18.6	1.301	F	2
J162424.80+574116.2	0.078	0.670	0.782	594.4	-0.08	0.000	19.7	0.789	F	1
J162432.18+565228.0	0.076	0.470	0.772	368.6	-0.20	0.000	17.8	–	B	3
J162435.71+274857.7	0.086	0.134	0.092	230.5	-1.43	0.000	–	–	?	0
J163041.81+070109.0	0.066	0.149	0.151	210.2	-0.42	0.000	18.8	0.736	F	2
J163116.54+492739.4	0.126	0.939	0.959	657.1	-0.42	0.034	18.4	0.520	F	1
J163638.18+211255.6	0.060	0.478	0.754	411.1	-0.01	0.000	18.7	1.791	F	2
J163813.45+572023.9	0.112	0.798	0.901	1338.2	-0.07	0.115	16.9	0.750	F	1
J164029.63+394646.0	0.138	–	–	1650.8	-0.33	0.000	18.7	1.660	F	1
J164125.23+225704.0	0.068	0.487	0.409	374.6	-0.12	0.013	19.5	2.046	F	2
J164207.85+685639.7	0.053	0.471	0.698	1206.2	0.18	0.025	19.3	0.751	F	1
J164258.80+394836.9	0.126	0.025	0.192	6299.8	0.05	0.325	16.8	0.593	F	1
J164656.86+405917.1	0.107	0.142	0.082	495.7	-0.36	0.000	19.3	0.835	F	1
J164801.53+222433.2	0.059	0.488	0.727	313.2	-0.10	0.000	–	–	?	0

Table 1—Continued

Name	FoM	Prod Prob	Peak Prob	S <sub>8.4</sub> (mJy)	$\alpha$	RASS Cnts	R2	z	Type <sup>a</sup>	ID Origin <sup>b</sup>
J165103.66+012923.4	0.069	0.834	0.405	663.9	0.00	0.000	–	–	?	0
J165201.40+061855.3	0.066	0.567	0.320	326.2	-0.15	0.000	20.0	–	?	0
J165258.50+390249.8	0.067	0.070	0.297	334.8	-0.14	0.000	20.5	–	?	0
J165329.90+310756.9	0.096	0.896	0.963	378.5	-0.38	0.023	14.7	1.298	F	1
J165518.79+423339.8	0.064	0.120	0.173	245.5	-0.28	0.000	20.4	–	?	0
J165802.78+473749.2	0.109	0.262	0.141	1186.4	-0.18	0.030	17.0	1.622	F	1
J165833.44+051516.4	0.084	0.368	0.451	1287.8	0.08	0.118	16.2	0.879	F	1
J170009.29+683006.9	0.065	0.502	0.190	383.5	-0.08	0.012	18.4	0.301	F	1
J170124.63+395437.0	0.068	0.520	0.661	285.4	-0.24	0.000	16.2	–	B	5
J170732.47+112200.7	0.089	0.130	0.354	270.0	-0.51	0.000	18.9	2.406	F	2
J170734.41+014845.6	0.063	0.164	0.254	467.6	-0.01	0.000	18.5	2.576	F	1
J170745.63+133105.2	0.103	0.070	0.172	458.8	-0.24	0.102	16.9	–	?	0
J171611.19+215213.6	0.065	0.500	0.754	605.8	0.02	0.000	18.9	0.358	F	2
J171613.93+683638.7	0.143	0.451	0.436	819.7	-0.30	0.119	17.6	0.777	F	1
J171913.04+174506.4	0.072	0.433	0.370	579.9	-0.04	0.027	17.2	0.137	B	2
J171914.49+485849.4	0.050	0.262	0.306	206.7	-0.20	0.056	9.44	0.024	N	1
J171938.25+480412.2	0.086	0.634	0.680	188.1	-0.61	0.120	14.2	1.083	F	1
J171952.20+081703.5	0.116	0.007	0.007	604.8	-0.37	0.000	15.8	1.185	F	2
J172109.49+354216.0	0.099	0.165	0.467	601.4	-0.24	0.060	16.9	0.283	F	1
J172236.72+585622.2	0.072	–	–	328.0	-0.21	0.000	19.0	1.979	F	1
J172414.19+330303.9	0.088	0.236	0.256	559.8	-0.17	0.020	19.8	1.870	F	1
J172504.34+115215.4	0.103	0.457	0.530	198.0	-0.29	0.870	14.4	0.018	B	1
J172635.12+321323.0	0.050	0.429	0.527	191.2	-0.27	0.000	17.2	1.094	F	1
J172704.55+052852.1	0.077	–	–	226.7	-0.50	0.000	19.9	–	?	0
J172723.46+551053.5	0.080	0.690	0.505	265.3	-0.35	0.080	–	0.247	N	1
J172727.64+453039.7	0.119	0.834	0.912	1360.3	-0.23	0.026	16.6	0.714	F	1
J172807.05+121539.4	0.059	0.287	0.117	365.0	-0.04	0.000	19.4	0.583	F	2
J173420.58+385751.4	0.114	0.323	0.726	1160.0	-0.22	0.011	19.0	0.970	F	1
J173549.00+504911.5	0.143	–	–	952.0	-0.45	0.000	–	–	?	0
J173548.08+361645.6	0.164	0.910	0.729	958.7	-0.59	0.037	18.7	0.803	F	1
J173628.58+063147.5	0.081	0.924	0.923	217.2	-0.84	0.000	–	2.387	F	2
J173840.50+322409.0	0.079	0.598	0.290	294.1	-0.34	0.000	14.8	0.126	F	1
J173927.39+495503.3	0.073	0.095	0.050	577.7	-0.05	0.025	17.8	1.545	F	1
J173935.36+335808.2	0.052	0.843	0.303	224.9	-0.18	0.000	–	1.625:	F	2
J173957.12+473758.3	0.085	0.046	0.237	833.0	-0.07	0.014	18.8	0.316	B	1
J174005.86+221100.9	0.092	0.492	0.765	512.6	-0.23	0.000	16.7	–	?	0
J174048.95+434816.1	0.083	0.297	0.352	257.0	-0.48	0.000	19.1	2.246	F	2
J174134.82+475132.5	0.075	0.015	0.056	201.2	-0.78	0.000	–	–	?	0
J174347.64+374753.8	0.104	0.742	0.271	430.0	-0.40	0.000	20.1	1.958	F	1
J174504.66+225248.0	0.053	0.137	0.082	246.0	-0.13	0.000	20.0	1.883	F	1
J174535.20+172001.4	0.054	0.700	0.776	806.8	0.14	0.000	18.2	1.702	F	1
J174726.64+465850.9	0.162	0.046	0.139	882.3	-0.60	0.016	19.1	1.484	B	1
J174805.82+340401.1	0.063	0.765	0.558	270.1	-0.20	0.000	19.1	2.763	F	2
J174832.83+700550.7	0.051	0.102	0.107	572.8	0.12	0.060	15.4	0.770	B	1
J175132.82+093900.7	0.186	0.005	0.075	2015.2	-0.67	0.000	15.5	0.322	F	1
J175246.00+173420.3	0.075	0.265	0.672	404.3	-0.14	0.071	15.9	0.507	F	1

Table 1—Continued

Name	FoM	Prod Prob	Peak Prob	S <sub>8.4</sub> (mJy)	$\alpha$	RASS Cnts	R2	z	Type <sup>a</sup>	ID Origin <sup>b</sup>
J175322.64+440945.6	0.081	0.358	0.210	810.4	-0.04	0.030	18.7	0.871	F	1
J175342.47+284804.9	0.077	0.174	0.230	499.4	-0.11	0.021	20.2	–	?	0
J175653.10+153520.8	0.136	0.219	0.145	503.8	-0.69	0.000	17.1	–	?	0
J175900.35+234346.9	0.050	0.318	0.431	567.0	0.12	0.014	15.7	1.721	F	1
J180024.76+384830.6	0.173	0.785	0.684	1211.2	-0.74	0.057	17.0	2.092	F	1
J180045.68+782804.0	0.117	–	–	2874.0	-0.15	0.066	15.4	0.680	F	1
J180408.88+004222.0	0.057	–	–	183.4	-0.05	0.362	13.8	–	?	0
J180415.98+010132.3	0.088	0.147	0.238	967.2	-0.07	0.000	17.3	1.522	F	1
J180547.43+171455.9	0.074	0.666	0.839	236.4	-0.43	0.000	–	–	?	0
J180650.68+694928.1	0.110	0.013	0.013	1595.5	0.00	0.154	11.3	0.050	B	1
J180738.80+220456.4	0.099	0.508	0.152	275.7	-0.81	0.000	16.3	–	?	0
J180821.88+454220.8	0.085	0.461	0.698	434.9	-0.22	0.000	19.2	0.830	F	1
J180945.33+184903.0	0.055	0.961	0.945	218.7	-0.23	0.000	18.8	0.928	F	2
J181333.41+061542.0	0.060	0.101	0.261	261.6	-0.19	0.000	17.4	–	?	0
J181337.26+295237.8	0.055	0.087	0.054	314.5	-0.05	0.000	18.9	1.366	F	2
J181830.51+501719.7	0.055	0.662	0.530	239.2	-0.18	0.000	19.6	1.395	F	2
J182314.10+793849.0	0.121	–	–	592.0	-0.42	0.000	16.0	0.224	F	1
J182407.07+565101.4	0.079	0.744	0.897	1193.1	0.08	0.098	16.4	0.663	F	1
J182921.25+051813.1	0.057	–	–	192.9	-0.36	0.000	–	–	?	0
J183005.93+061915.9	0.070	–	–	452.6	-0.08	0.000	–	–	?	0
J183243.47+135744.4	0.094	0.029	0.050	819.7	-0.14	0.000	18.1	–	?	0
J183519.67+611940.0	0.052	0.588	0.412	486.6	0.08	0.009	18.0	2.274	F	1
J183558.38+250645.4	0.067	0.087	0.508	180.6	-0.98	0.000	15.9	1.972	F	1
J183700.72+750732.5	0.079	–	–	267.6	-0.40	0.009	20.3	–	?	0
J184003.44+245741.2	0.052	0.006	0.061	162.2	-0.48	0.000	19.5	1.634	F	2
J184057.16+390045.7	0.060	0.981	0.972	227.8	-0.26	0.000	19.1	3.095	F	1
J184233.64+680925.2	0.082	0.141	0.277	846.7	-0.05	0.051	18.0	0.475	F	1
J184631.92+374717.3	0.056	0.661	0.697	202.8	-0.31	0.000	18.9	2.441	F	2
J184712.65+081035.3	0.052	–	–	226.3	-0.17	0.000	–	–	?	0
J184822.10+321902.5	0.091	0.088	0.290	640.5	-0.13	0.075	18.7	0.798	F	2
J184916.07+670541.6	0.058	0.256	0.289	476.0	0.03	0.031	17.4	0.657	F	1
J184920.10+302414.1	0.051	0.025	0.028	255.8	-0.09	0.000	19.4	–	?	0
J185027.59+282513.1	0.180	0.011	0.067	1527.4	-1.06	0.000	17.1	2.560	F	1
J185230.37+401906.5	0.061	0.728	0.797	583.6	0.04	0.000	19.0	2.120	F	1
J185228.55+485547.4	0.082	0.140	0.444	374.1	-0.26	0.000	18.7	1.250	F	1
J185457.29+735119.9	0.099	0.099	0.173	600.3	-0.24	0.067	16.3	0.460	F	1
J185527.71+374256.9	0.050	0.368	0.663	227.6	-0.14	0.000	–	1.120	F	2
J190414.36+153638.4	0.066	–	–	349.8	-0.12	0.000	20.4	–	?	0
J191810.74+552038.6	0.081	0.698	0.638	424.6	-0.20	0.000	19.1	1.734	F	2
J191845.57+493756.0	0.050	0.605	0.662	213.3	-0.18	0.000	17.4	–	?	0
J192439.45+154043.9	0.062	–	–	387.8	-0.05	0.000	–	–	?	0
J192559.60+210626.1	0.100	–	–	1414.7	-0.10	0.000	16.1	–	?	0
J192730.44+611732.8	0.063	0.185	0.121	514.0	0.00	0.021	16.9	–	B	5
J192748.49+735801.5	0.130	0.459	0.520	3697.8	0.02	0.277	15.1	0.360	F	1
J192904.58+232529.2	0.078	–	–	291.5	-0.33	0.000	–	–	?	0
J193357.33+654016.8	0.061	0.988	0.972	285.6	-0.15	0.012	20.0	–	?	0

Table 1—Continued

Name	FoM	Prod Prob	Peak Prob	S <sub>8.4</sub> (mJy)	$\alpha$	RASS Cnts	R2	z	Type <sup>a</sup>	ID Origin <sup>b</sup>
J193510.47+203154.1	0.081	–	–	505.3	-0.14	0.000	–	–	?	0
J193522.68+813014.5	0.052	–	–	294.9	-0.04	0.000	–	–	?	0
J193603.55+713131.7	0.057	0.256	0.536	497.0	0.04	0.000	18.4	1.864	F	1
J193951.81+371330.4	0.062	–	–	351.2	-0.08	0.000	17.8	–	?	0
J194943.48+504131.9	0.069	0.769	0.647	308.7	-0.20	0.000	15.5	1.929	F	2
J195330.87+353759.3	0.117	–	–	628.0	-0.37	0.000	16.7	–	?	0
J195455.98+615358.2	0.070	–	–	186.7	-0.64	0.000	–	–	?	0
J195511.57+135816.2	0.087	–	–	310.1	-0.39	0.000	18.5	–	?	0
J195542.73+513148.5	0.099	0.609	0.402	1822.6	-0.08	0.036	17.3	1.220	F	1
J195555.26+061812.1	0.061	0.561	0.337	190.1	-0.44	0.000	14.9	–	?	0
J195959.84+650854.6	0.071	–	–	222.8	0.04	2.653	11.2	0.048	B	1
J200210.41+472528.7	0.116	–	–	849.3	-0.28	0.008	19.6	–	?	0
J200252.09+450608.3	0.099	–	–	493.7	-0.30	0.000	–	–	?	0
J200417.12+735506.0	0.056	0.714	0.547	193.4	-0.35	0.000	–	–	?	0
J200530.99+775243.2	0.181	–	–	2674.8	-0.55	0.032	17.3	0.342	B	1
J200711.91+063644.5	0.055	0.251	0.057	287.7	-0.09	0.000	17.5	–	?	0
J200728.77+660722.5	0.060	0.731	0.609	480.9	0.01	0.000	20.3	1.325	F	1
J200744.94+402948.6	0.116	–	–	3247.0	-0.15	0.000	–	1.736	F	1
J200952.30+722919.3	0.061	0.912	0.872	791.9	0.09	0.000	19.4	–	B	5
J200955.50+072713.6	0.051	0.091	0.067	283.0	-0.04	0.000	19.7	0.762	F	2
J201049.29+611615.1	0.068	0.651	0.856	329.5	-0.16	0.000	17.7	–	?	0
J201205.63+462855.7	0.099	–	–	587.2	-0.00	0.234	15.4	–	G	2
J201528.82+341039.4	0.069	–	–	796.1	0.03	0.000	–	–	?	0
J201555.37+655452.6	0.054	0.438	0.341	553.6	0.09	0.000	19.0	2.845	F	1
J201613.85+163234.1	0.109	0.416	0.453	603.5	-0.32	0.000	17.2	–	?	0
J202135.27+051504.7	0.075	0.080	0.156	423.8	-0.14	0.000	17.8	–	S	2
J202206.68+613658.8	0.131	0.249	0.466	3131.0	-0.24	0.000	17.5	0.227	N	1
J202235.58+761126.1	0.054	–	–	400.0	0.02	0.000	17.5	–	B	5
J202319.01+315302.3	0.095	–	–	3480.4	-0.03	0.000	19.0	–	?	0
J202323.16+222352.5	0.057	–	–	302.9	-0.09	0.000	–	–	?	0
J202355.84+542735.8	0.082	–	–	1095.7	-0.01	0.017	20.3	–	?	0
J202509.63+031644.4	0.052	0.027	0.220	381.8	0.03	0.000	20.0	2.210	F	1
J203837.03+511912.6	0.058	–	–	4289.5	0.18	0.000	19.2	1.686	F	1
J204753.79+534332.3	0.055	–	–	348.5	-0.01	0.000	18.2	–	?	0
J205051.12+312727.3	0.059	–	–	630.5	0.07	0.000	–	3.180	F	1
J205135.58+174336.9	0.063	0.312	0.089	425.7	-0.03	0.000	14.4	–	?	0
J210138.83+034131.3	0.095	0.374	0.378	785.7	-0.15	0.028	17.6	1.013	F	1
J210156.67+200316.9	0.066	0.481	0.413	244.0	-0.30	0.000	17.6	–	?	0
J210243.81+675819.8	0.072	0.747	0.572	202.1	-0.54	0.000	–	–	?	0
J210610.82+213536.0	0.074	0.629	0.360	294.7	-0.28	0.000	20.2	0.646	F	1
J210628.15+023137.8	0.079	0.937	0.930	219.9	-0.55	0.000	19.3	2.942	F	2
J210841.03+143027.0	0.052	0.430	0.178	373.5	0.03	0.000	19.8	2.017	F	2
J210931.87+353257.6	0.088	–	–	891.8	0.15	0.372	13.9	–	?	0
J211440.64+171422.3	0.068	0.315	0.181	182.7	-0.98	0.000	–	–	?	0
J211458.33+283257.2	0.076	0.534	0.068	477.9	-0.11	0.000	18.9	2.345	F	2
J211529.41+293338.3	0.098	0.637	0.292	959.8	-0.14	0.011	19.2	1.514	F	1

Table 1—Continued

Name	FoM	Prod Prob	Peak Prob	S <sub>8.4</sub> (mJy)	$\alpha$	RASS Cnts	R2	z	Type <sup>a</sup>	ID Origin <sup>b</sup>
J212344.51+053522.0	0.136	0.358	0.610	1426.3	-0.33	0.027	19.8	1.878	F	1
J213638.58+004154.1	0.159	0.725	0.864	6725.4	-0.37	0.075	17.0	1.941	F	1
J213901.31+142335.9	0.152	0.295	0.408	2237.5	-0.39	0.000	18.2	2.469	F	1
J213942.50+012227.1	0.061	0.556	0.755	244.3	-0.24	0.000	18.9	1.401	F	1
J214710.16+092946.6	0.085	0.109	0.075	1002.0	-0.05	0.000	16.5	1.112	F	1
J214805.45+065738.6	0.225	0.124	0.369	7026.8	-0.59	0.114	15.0	0.990	F	1
J215131.42+070926.7	0.066	0.117	0.208	784.7	0.05	0.000	16.3	1.364	F	1
J215137.87+055212.9	0.057	0.111	0.351	577.8	0.07	0.000	–	0.740	F	1
J215224.82+173437.7	0.064	0.511	0.141	628.4	0.03	0.000	17.9	–	B	5
J215712.86+101424.7	0.055	0.032	0.004	322.3	-0.04	0.029	16.6	0.761	F	1
J215728.82+312701.3	0.074	0.817	0.812	490.0	-0.09	0.000	20.1	1.486	F	2
J220049.41+023430.0	0.051	0.168	0.605	172.3	-0.39	0.000	17.2	1.323	F	2
J220143.53+504856.3	0.079	–	–	811.5	-0.03	0.028	18.7	1.899	F	2
J220312.62+675047.6	0.113	–	–	340.8	-0.63	0.000	18.5	–	?	0
J220314.97+314538.2	0.155	0.654	0.787	2969.3	-0.09	0.242	14.3	0.298	F	1
J220326.89+172548.2	0.133	0.033	0.004	1088.6	-0.36	0.035	14.7	1.075	F	1
J220330.95+100742.5	0.067	0.034	0.006	223.6	-0.38	0.000	–	–	?	0
J220421.10+363237.1	0.103	0.500	0.741	295.5	-0.77	0.000	12.8	0.073	G	1
J220719.78+004157.3	0.056	0.127	0.273	229.1	-0.22	0.000	19.7	1.892	F	1
J220921.49+515801.8	0.084	–	–	423.4	-0.22	0.000	18.4	–	?	0
J221051.66+201324.0	0.080	0.343	0.144	252.9	-0.45	0.000	–	–	?	0
J221153.89+184149.9	0.156	0.067	0.041	307.4	-0.75	0.241	11.9	0.069	F	1
J221405.69+373909.2	0.066	0.977	0.960	279.7	-0.21	0.000	18.9	2.249	F	2
J221620.00+351814.1	0.109	0.942	0.790	636.5	-0.30	0.000	17.5	0.510	F	1
J221700.82+242146.0	0.075	–	–	583.7	-0.06	0.027	19.2	0.505	B	2
J221810.92+152035.7	0.127	0.132	0.172	428.8	-0.76	0.000	19.3	2.335	F	2
J221914.09+180635.5	0.107	0.166	0.350	377.9	-0.49	0.000	19.9	1.802	F	2
J221949.74+261327.9	0.115	0.963	0.713	427.0	-0.41	0.085	11.3	0.085	F	1
J222318.09+624933.7	0.052	–	–	196.1	-0.28	0.000	–	–	?	0
J222538.05+211806.4	0.074	0.252	0.456	1396.0	0.14	0.130	17.6	1.959	F	1
J223036.46+694628.0	0.106	0.122	0.274	767.9	-0.24	0.000	20.1	–	?	0
J223622.46+282857.4	0.146	0.998	0.922	2074.2	-0.35	0.000	17.6	0.795	F	1
J223638.59+732252.6	0.072	0.421	0.299	357.6	-0.17	0.000	19.9	1.345	F	1
J223810.39+072413.9	0.112	0.694	0.406	337.4	-0.68	0.000	18.1	1.011	F	2
J223812.87+274952.7	0.052	0.989	0.979	178.9	-0.37	0.000	18.8	0.835	F	2
J223815.03+680459.7	0.068	–	–	225.1	-0.38	0.000	19.3	–	?	0
J223819.30+041231.5	0.080	0.973	0.979	213.4	-0.65	0.000	16.5	1.009	F	2
J224107.20+412011.6	0.146	0.602	0.186	825.6	-0.51	0.000	18.8	–	B	3
J224149.71+095352.4	0.087	0.176	0.220	607.3	-0.15	0.000	18.0	1.707	F	1
J224435.15+260020.7	0.067	0.831	0.565	188.2	-0.55	0.000	18.8	2.042	F	2
J224528.28+032408.8	0.092	0.644	0.564	643.8	-0.17	0.000	17.5	1.340	F	1
J224758.67+031042.3	0.073	0.658	0.561	783.8	0.00	0.000	19.7	–	?	0
J224900.56+210702.8	0.068	0.262	0.448	717.5	0.02	0.000	–	1.274	F	2
J225042.84+555014.6	0.060	–	–	405.4	-0.02	0.000	16.7	–	?	0
J230042.99+165514.3	0.076	–	–	406.9	-0.16	0.000	–	1.284	F	2
J230241.31+640552.8	0.071	–	–	219.4	-0.45	0.000	–	–	?	0



Table 1—Continued

Name	FoM	Prod Prob	Peak Prob	S <sub>8.4</sub> (mJy)	$\alpha$	RASS Cnts	R2	z	Type <sup>a</sup>	ID Origin <sup>b</sup>
J230715.91+323031.9	0.077	0.487	0.838	679.3	-0.05	0.000	19.6	1.937	F	2
J230734.00+145017.9	0.077	0.494	0.699	239.7	-0.45	0.000	19.3	0.503	N	2
J230811.63+200842.2	0.054	0.074	0.224	240.7	-0.15	0.068	16.5	0.234	F	1
J231147.40+454356.0	0.104	–	–	614.3	-0.27	0.000	19.1	1.447	F	1
J232220.35+444542.3	0.051	–	–	347.0	0.01	0.000	–	1.310:	F	2
J232225.97+505751.9	0.109	–	–	1676.8	-0.15	0.000	18.5	1.279	F	2
J232228.56+184324.9	0.050	0.117	0.181	323.0	0.01	0.000	18.5	1.728	F	2
J232721.96+152437.3	0.053	0.517	0.262	251.1	-0.13	0.000	10.0	0.046	F	1
J232733.57+094009.4	0.061	0.588	0.786	652.7	0.06	0.056	18.2	1.843	F	2
J232735.98+153309.5	0.093	0.541	0.330	256.3	-0.85	0.000	17.2	0.989	F	1
J233013.73+334836.4	0.119	0.472	0.293	473.5	-0.49	0.000	18.7	1.809	F	1
J233040.85+110018.7	0.052	0.444	0.521	884.1	0.16	0.025	18.2	1.488	F	1
J233412.82+073627.5	0.119	0.545	0.651	922.2	-0.23	0.082	16.4	0.401	F	2
J234312.38+233945.6	0.074	0.376	0.469	442.7	-0.12	0.000	18.4	–	?	0
J234342.75+154302.9	0.076	0.586	0.523	273.2	-0.35	0.000	19.7	1.441	F	4
J234636.83+093045.5	0.064	0.047	0.149	1337.4	0.16	0.090	15.9	0.677	F	1
J234625.57+800755.2	0.052	–	–	208.7	-0.22	0.000	19.5	–	?	0
J235248.91+394756.2	0.058	–	–	247.1	-0.19	0.000	–	1.682:	F	2
J235342.30+551840.6	0.093	–	–	393.9	-0.33	0.000	18.8	1.927	F	2
J235622.79+815252.2	0.065	–	–	517.3	-0.00	0.000	17.9	1.344	F	1

Note. —  $\gamma$ -ray probabilities are only listed for sources that survive our spatial cuts. Uncertain redshifts are denoted by trailing ':'.

<sup>a</sup>USNO B1.0 R2 magnitude

<sup>b</sup>Classification: F = FSRQ, B = BL Lac, N = NLRG, ? = UNIDED.

<sup>c</sup>Origin of Spectroscopy: 0 = No info, 1 = Archival, 2 = Our McDonald Observatory spectroscopy, 3 = Our McDonald Observatory spectroscopy of a featureless BL Lac, 4 = Our McDonald Observatory spectroscopy in addition to archival data, 5 = Archival featureless BL Lac

Table 2. X-ray Selected Targets

Name(J2000)	$z$	Type <sup>a</sup>
J064501.37+602442.3	0.8319	f
J073502.30+711506.4	0.7950	f
J074129.61+255733.8	2.7425	f
J081108.33+573024.0	0.4180	n
J085749.78+013531.7	0.2818	b
J085930.71+621730.4	–	b
J090147.03+655150.1	2.0720	f
J091925.68+110657.2	0.4232	b
J093239.30+104231.3	–	b
J094836.94+220053.4	0.7152	f
J094935.10+232927.0	0.6621	f
J095359.22+172056.8	0.7110	f
J100800.83+062121.7	–	b
J102839.53+170211.0	–	b
J103144.81+602030.2	1.2284	f
J103633.02+220312.1	0.5950	f
J104418.48+603701.1	1.0502	f
J111118.57+153030.1	0.5252	f
J113245.64+003427.9	–	b
J113255.95+051538.5	0.1003	b
J114803.48+565408.3	0.4503	f
J115409.25+023816.5	0.2122	f
J120127.32+090039.7	1.0125	f
J122339.24+461119.5	1.0096	f
J122401.04+223938.9	–	b
J122916.22+042319.5	1.0260	f
J124509.97+570954.6	–	b
J124709.63+324703.8	0.1348	n
J124834.32+512807.6	0.3501	b
J131930.32+485103.8	1.1702	f
J133133.36+171249.7	–	b

Table 2—Continued

Name(J2000)	$z$	Type <sup>a</sup>
J134136.07+551439.4	0.2073	b
J134541.62+312406.4	0.2228	e
J134737.29+301255.5	0.1170	f
J135013.50+712548.5	0.4871	n
J135120.91+111452.6	–	b
J135738.69+012813.4	0.2187	b
J140655.86+582200.5	0.2861	n
J141959.25+270626.6	0.5357	f
J142421.06+370553.7	0.2888	b
J142455.48+361536.3	–	b
J143825.50+120419.5	–	b
J144053.02+061015.4	–	b
J150644.48+081358.6	–	b
J151039.47+312716.0	0.6722	f
J152913.33+381217.1	–	b
J153137.07+085242.3	0.1585	e
J153149.18+465914.7	0.3163	b
J153208.90+585422.6	0.0679	e
J153449.35+652847.8	0.5393	f
J160618.39+134530.6	0.2942	b
J161826.96+081950.7	0.4453	f
J162358.20+074130.0	1.2965	f
J162839.13+252756.0	0.2202	b
J163319.74+211253.2	0.1982	f
J165221.57+493255.5	–	b
J165201.52+623208.5	1.6296	f
J170112.38+353350.8	0.5004	f
J171531.53+205935.5	0.1773	e
J172242.00+281459.2	0.9495	f
J173328.83+451951.0	0.3171	b
J174816.01+494148.2	0.1879	e

Table 2—Continued

Name(J2000)	$z$	Type <sup>a</sup>
J211353.23+133017.2	0.3073	b
J215218.83+190150.9	0.7077	f
J221130.56+291948.8	0.1492	f
J221950.94+073643.4	0.6108	f
J224456.10+105611.6	0.2467	n
J225515.34+241012.4	–	b
J231217.01+161508.0	1.2733	f
J231357.26+144422.5	0.1625	b
J232046.75+182925.5	0.7348	f
J232733.57+094009.1	1.8536	f
J233412.80+073626.9	0.4011	f
J234631.61+402416.1	0.0838	f

<sup>a</sup>Classification: f = FSRQ, b = BL Lac, n = NLRG, e = Passive Elliptical

Table 3.  $\gamma$ -ray Probability Distribution

	#Prob<0.005	<0.01	<0.05	<0.1
Peak	4	6	34	68
Product	0	8	41	79
Random	2.9	5.8	28.8	57.6